The Effect of Compositional and Geometrical Changes to the Bending Strength of the Ghanaian Ceramic Pot Filter

by

Travis Watters

SUBMITTED TO THE DEPARTMENT OF CIVIL AND ENVIRONMENTAL ENGINEERING IN PARTIAL FULFILLMENT OF THE REQUIREMENTS FOR THE DEGREE OF

MASTERS OF ENGINEERING IN CIVIL AND ENVIRONMENTAL ENGINEERING
AT THE
MASSACHUSETTS INSTITUTE OF TECHNOLOGY

JUNE 2010

© Travis Watters. All rights reserved.

The author hereby grants to MIT permission to reproduce
and to distribute publicly paper and electronic
copies of this thesis document in whole or in part
in any medium now known or hereafter created.

Signature of Author: _____
Department of Civil and Environmental Engineering
May 21, 2010

Certified by: _____
Susan Murcott
Senior Lecturer of Civil and Environmental Engineering
Thesis Supervisor

Accepted by: _____
Daniele Veneziano
Chairman, Departmental Committee for Graduate Students

The Effect of Compositional and Geometrical Changes to the Bending Strength of the Ghanaian Ceramic Pot Filter

by
Travis Watters

Submitted to the Department of Civil and Environmental Engineering on May 21, 2010, in Partial Fulfillment of the Requirements for the Degree of Masters of Engineering in Civil and Environmental Engineering

ABSTRACT

Pure Home Water (PHW) is a non-profit organization with the goal of providing safe drinking water through household water treatment and storage (HWTS) to the inhabitants of Ghana, particularly in the Northern Region. To this end, PHW has pursued the distribution and training in the use of the *Kosim* ceramic pot filter (CPF), and now wishes to pursue its manufacture. Laboratory studies have found the CPF to be between 97.8 and 100% efficient in the removal of *E. coli* bacteria.

One of the main reasons for a household's discontinued use of the CPF is breakage. In a follow-up monitoring of 1,000 homes receiving CPFs after an emergency flood distribution in 2008, the rate of breakage was found to be 12%. To address this critical problem, the author performed a three-point bending test on rectangular-prism clay samples with varying recipes and thicknesses in an attempt to determine bending strengths associated with the recipes with the aim of moderating the lip failure due to the possible failure mechanism of bending stress.

Filter recipes were assigned numbers 1 through 14 based on combustible type, presence or absence of grog, combustible volume, and manufacturing process. The recipes which incorporated only fine, sieved combustible materials yielded the highest mean bending strengths. Statistically significant decreases in bending strength were realized with the increase of combustible mass. The inclusion of grog was generally found to have no statistically significant impact on the bending strength. Experimentally observed gains in bending strength with increased thickness supported theoretical strength gains with the square of the thickness. The variable of firing condition was found to be a significant but unquantifiable variable in the bending strength of the samples. In all cases, the lower bound of a 95% confidence interval of the mean bending strength of the materials was found to exceed the expected bending stress on the filter lip due to predicted loading conditions.

It is recommended that PHW pursue the manufacture of a fine-and-waste rice husk recipe with a 3:8 combustible-to-clay ratio without the inclusion of grog. It is recommended that the lip of the filter be thickened to 25 mm. It is recommended that pyrometric cones be placed in the spyhole and door of the kiln during each firing and monitored once an hour until the guide cone bends, and once every fifteen minutes thereafter until the firing cone bends, at which time firing should cease. It is recommended that consultation with kiln designer Manny Hernandez be maintained so as to create even firing conditions within the kiln.

Thesis Supervisor: Susan Murcott

Title: Senior Lecturer of Civil and Environmental Engineering

ACKNOWLEDGEMENTS

I wish to thank the following people for their assistance in completing this thesis.

Susan Murcott, fellow traveler and advisor. To say that without her, this thesis would be impossible, is to state an obvious truth. It is because of her work in founding Pure Home Water and her career in the developing world in general that I have had the unspeakable good fortune to travel the world and leverage my efforts in support of the needy and unseen.

Manny Hernandez, fellow traveler, kiln/press designer/builder, and overall benchmark-setter for toughness, discipline, and dedication. I have never seen a person work so hard or so consistently or with such enthusiasm. If I can be half the man he is one day I'll be at least twice the man I am now.

Reed Miller, fellow traveler, research partner, ceaseless do-gooder, and Manny Hernandez-style worker. Our theses were mutually dependent, but I have no doubt that he would have done the work of both of us if I hadn't been there.

Thomas Hay and Leah Nation, fellow travelers, therapists, and facilitators. Despite having their own projects to manage, each was instrumental in the implementation of mine. I couldn't have done it without them and it wouldn't have been any fun if I had tried.

Zainab, Mildred, Ruben, Mr. Sabani, Mr. John, and the rest of the Pure Home Water employees who kept us running with food, equipment, leadership, and encouragement whenever the aforementioned were in short supply.

The men and women of Taha, whose staggering physical endurance left me grateful and downright shamed.

Stephen Rudolph, who wrote the program and provided the equipment and instruction necessary for me to perform an outlandish number of three-point bending tests.

Dr. J. J. Connor and Dr. Ezra Glen, who, in the eleventh hour, advised this poor environmental engineer when the structural and statistical waters threatened to overwhelm him.

Michael Shearer, for sympathetically pacing me through the nitty-gritty structural calculations, and whose alarming tech savvy facilitated the snazzy 3-D renderings that otherwise would have been the disappointing result of many an hour's clumsy labor.

All of my fellow MEng professors and colleagues, whose past and ongoing accomplishments inspire me to be worthy of their company.

And of course, Mom and Dad, who love me thesis or no. So much of my work is attributable to you, since I wouldn't be the person I am without you. You are therefore accessories to both my failures and triumphs; let us hope this is one of the latter.

Table of Contents

Table of Figures

1 Introduction

1.1 The Necessity of Safe Drinking Water

The importance of safe drinking water[1] for the maintenance of human health is well-documented. The World Health Organization (WHO) estimates approximately 1.8 million deaths occur annually due to diarrheal diseases (WHO, 2004, p. 120). Nath, Bloomfield, and Jones estimate that 88% of these deaths are due to unsafe water supply, inadequate sanitation, and hygiene, and that 99.8% of water and sanitation-related deaths occur in developing countries (2006, p. 9).

The United Nations (UN) 2009 Millenium Development Goals (MDG) Report claims 884 million people still rely on unimproved water sources[2] for drinking, cooking, bathing, and other domestic uses (UN, 2009, p. 46). Furthermore, the 2009 MDG Report admits that improved water sources[3] do not always provide safe drinking water; many samples taken from improved sites have failed to meet the microbiological standards put forth by WHO (UN, 2009, p. 47).

Access to improved water sources is particularly low in rural areas. Eighty-four per cent of those without access to improved water sources live in rural areas (UN, 2009, p. 46). Approximately 27% of the world's rural population enjoys access to piped water, while approximately 50% rely on other improved sources, leaving approximately 24% to depend on unimproved sources (UN, 2009, p. 47). Figure 1-1 provides a more detailed representation of the rural population's water sources.

[1] "Safe drinking water" is here defined as water meeting the requirements found in the World Health Organization's Guidelines for Drinking-water Quality, Incorporating First and Second Addenda to Third Edition: Volume 1, Recommendations. The full text of this document is available online at http://www.who.int/water_sanitation_health/dwq/fulltext.pdf

[2] WHO and the the United Nations International Children's Emergency Fund (UNICEF) define unimproved water sources as: unprotected dug wells, unprotected springs, carts with small tank/drum, tanker trucks, surface water, and bottled water (WHO/UNICEF, 2008, p.22).

[3] WHO/UNICEF separates improved water sources into two categories: water piped into a dwelling, plot, or yard; and "other improved sources," which includes public taps or standpipes, tube wells or boreholes, protected dug wells, protected springs, and rainwater collection (WHO/UNICEF, 2008, p. 22).

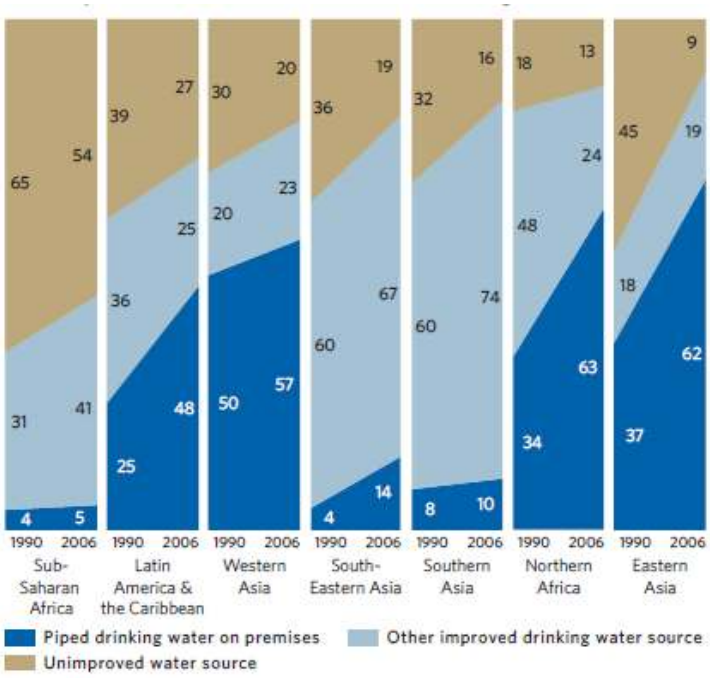

Figure 1-1: Percentage of Rural Households Using Piped Water, Other Improved Sources, and Unimproved Sources, 1990 and 2006 (UN, 2009, p. 46).

1.2 Background Information

The impetus of this thesis is the desire to improve the ceramic pot filters (CPFs) used by Pure Home Water (PHW), a non-profit organization in the Northern Region of Ghana. It is therefore instructive to provide background information on Ghana, CPFs, and PHW.

1.2.1 Ghana

The country of Ghana in Western Africa is highlighted in Figure 1-2. It possesses a tropical climate, a population of 23.9 million, and a land area (239,460 km^2) slightly less than that of Oregon (Central Intelligence Agency [CIA], 2009).

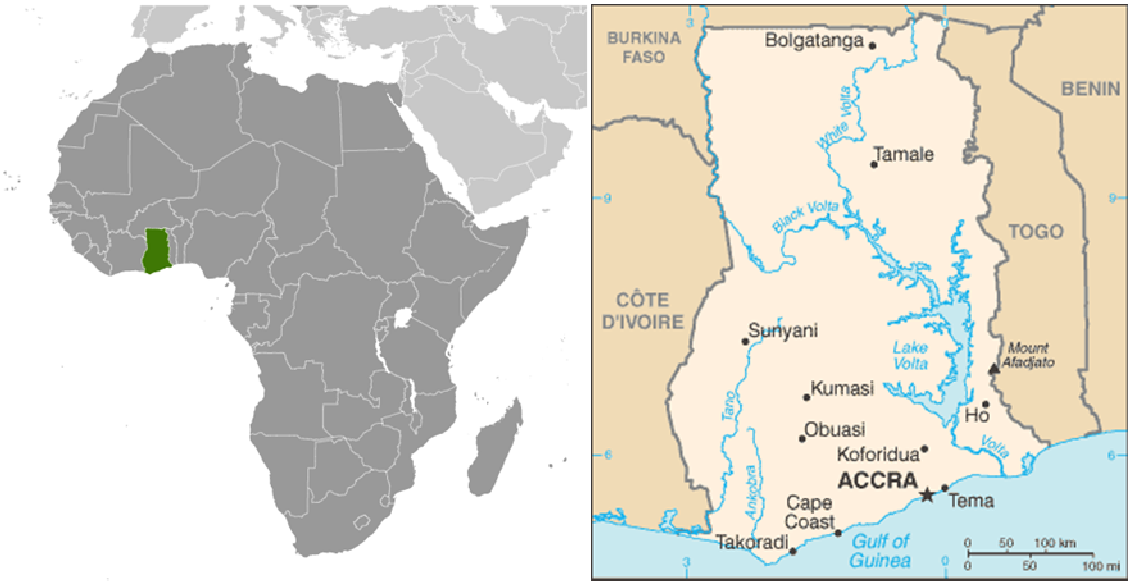

Figure 1-2: Map of Africa (Left); Map of Ghana (Right) (CIA 2009)

1.2.1.1 Under-Five Mortality

As of 2006, the United Nation's International Children's Fund (UNICEF) estimates Ghana's under-five mortality rate at 120 deaths per 1,000 live births – the 32nd highest in the world (UNICEF, State of the World's Children, 2007, p. 113). According to 2003 statistics, an estimated 12% of deaths under five in Ghana are due to diarrheal diseases (WHO, 2006). As mentioned in Section 1.1, diarrheal diseases are strongly correlated to unsafe water supply, inadequate sanitation, and hygiene.

The country is divided into ten administrative divisions known as Regions (CIA, 2009). In the Northern Region – the area of focus for this thesis – the under-five mortality rate is significantly higher than the national average, at 154 deaths per 1,000 live births. Were the Northern Region its own country, its under-five mortality rate would be the 19th highest in the world (UNICEF, 2007, p. 113). Figure 1-3 presents a graphical representation by region of the under-five mortality rates in Ghana.

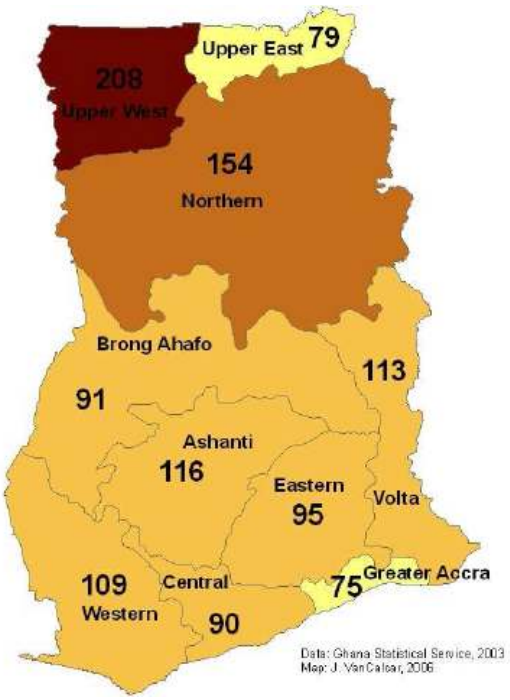

Figure 1-3: Under-Five Mortality Rates Per 1,000 Live Births in Ghana, 2003: (Van Calcar, 2006, p. 17)

1.2.1.2 Drinking Water Coverage

Given WHO's estimate that 12% of Ghana's under-five deaths are attributable to diarrhea, and Nash, Bloomfield, and Jones's estimate that 88% of diarrheal deaths are attributable unsafe water supply, inadequate sanitation, and hygiene, data pertaining to Ghana's water supply coverage is of interest. As of 2006, 29% of rural Ghanaians still lacked access to improved water sources (WHO/UNICEF, 2008, p. 45). Table 1-1 describes the distribution of drinking water access in Ghana in more detail.

Table 1-1: Drinking Water Coverage in Ghana, 2006

	Improved	Piped Connection	Other Improved	Unimproved
Urban	90%	37%	53%	10%
Rural	71%	4%	67%	29%
Total	80%	20%	60%	20%

(Adapted from WHO/UNICEF, 2008, p. 45)

As of 2003, 900,000 of the 1.8 million people living in Ghana's Northern Region lacked access to improved water sources (Ghana Statistical Service, 2005). Figure 1-4 provides graphical information as to the distribution of improved and unimproved water access in the Northern Region.

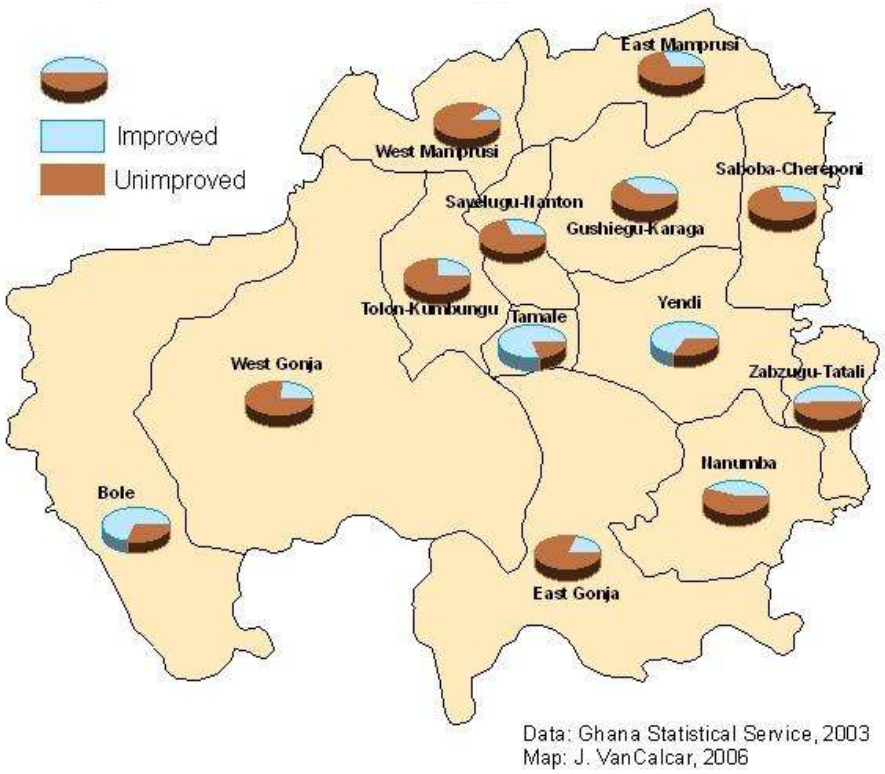

Figure 1-4: Percentage Use of Improved and Unimproved Drinking Water Sources in the Northern Region of Ghana (Van Calcar, 2006, p. 25);

1.2.1.3 Unimproved Water Quality

For those Ghanaians using unimproved water sources, it is useful to have an idea of the quality of their water. For many residents in the Northern Region, the water source is simply a dugout[4] of the kind pictured in Figure 1-5.

[4] "Dugout" is a term used locally in Ghana to refer to either (1) a pit dug into the ground for the collection of rainwater, or (2) a dammed reservoir for the storage of rainwater and streamwater.

Figure 1-5: Women at the Taha Dugout, Northern Region, Ghana

Murcott provides the following data, presented in Figure 1-6, for *E. coli* contamination in selected Ghanaian dugouts:

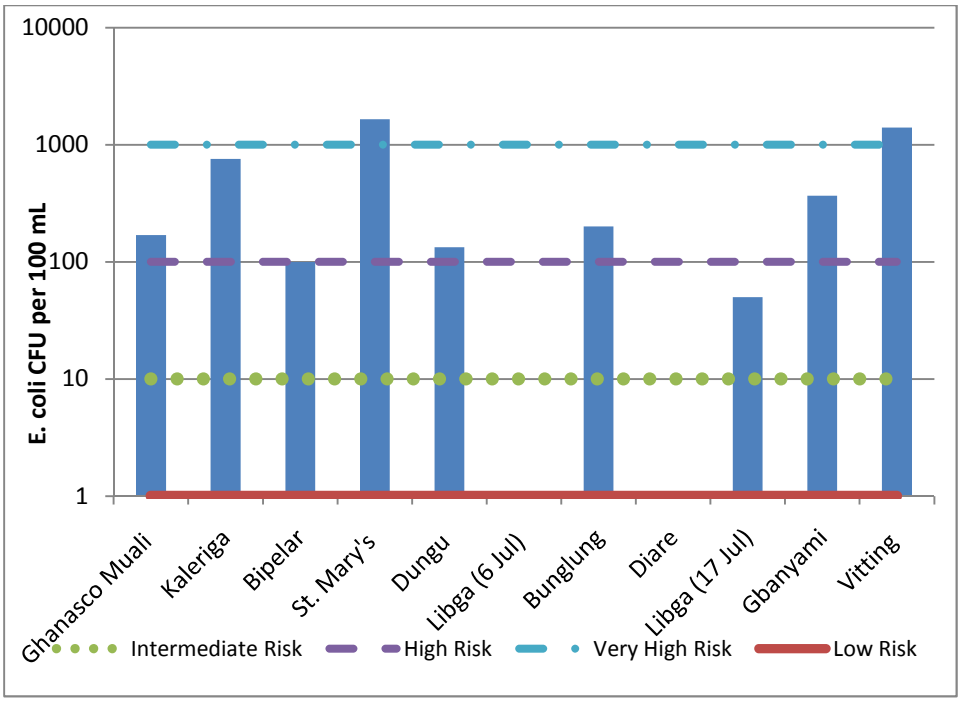

Figure 1-6: *E. coli* Contamination in Selected Ghanaian Dugouts, 2006 (Adapted from Murcott, 2009)

For purposes of comparison, the bottom boundary of WHO's water quality risk levels are graphed along with the measured data (WHO, 1997). One sees that all dugouts except Libga and Diare are classified, at best, as high risk.

1.2.2 Pure Home Water

To combat the lack of safe drinking water in Northern Ghana, Susan Murcott, Senior Lecturer at the Massachusetts Institute of Technology (MIT) founded the non-profit organization Pure Home Water (PHW) in cooperation with local Ghanaian partners in 2005 (Murcott, 2009). The organization has two stated goals:

1. Provide safe water via household drinking water treatment and safe storage products to Ghanaians in need of safe drinking water, with special emphasis on the region of Northern Ghana.

2. Become locally self-sufficient and financially self-supporting.

(Pure Home Water, 2009)

During its first five years, PHW focused on distribution, training, and monitoring of CPFs. In order to more efficiently meet its stated goals, PHW has decided to pursue the local manufacture of CPFs as well.

1.2.3 Ceramic Pot Filters

1.2.3.1 A Brief History of the Ceramic Pot Filter

The dissemination of CPFs was set in motion in 1998, when a non-profit organization known as Potters for Peace (PFP) adopted a filter invented in 1981 by Dr. Fernando Mazariegos of the Central American Industrial Research Institute (Potters for Peace, 2006). At this time, the general filtering capability of ceramics was well known; The Royal Doulton Company has been manufacuring ceramic candle filters since John Doulton first built a stoneware unit with a clay filter element for Queen Victoria in 1835 (DoultonUSA, 2010). However, the CPF was a definitive innovation in terms of cost, ease of use, and potential for local production almost anywhere in the world. When Hurricane Mitch hit Central America in 1998, PFP initiated the Filtron workshop in Nicaragua for the production of Mazariegos's filters (Potters for Peace, 2006). Since then, at least 35 filter factories have been established in at least 18 different countries worldwide (Rayner, 2009, p. 55).

1.2.3.2 The Kosim Ceramic Pot Filter

Each country has its own version of the PFP filter. The model adopted by PHW is known locally as *Kosim* – a word which in the Northern Region's Dagbani language means "water from a ceramic pot" and "the best water" (Ziff, 2009, p. 18). Figure 1-7 contains photographs of the *Kosim* filter produced by Ceramica Tamakloe Ltd. in Accra, Ghana.

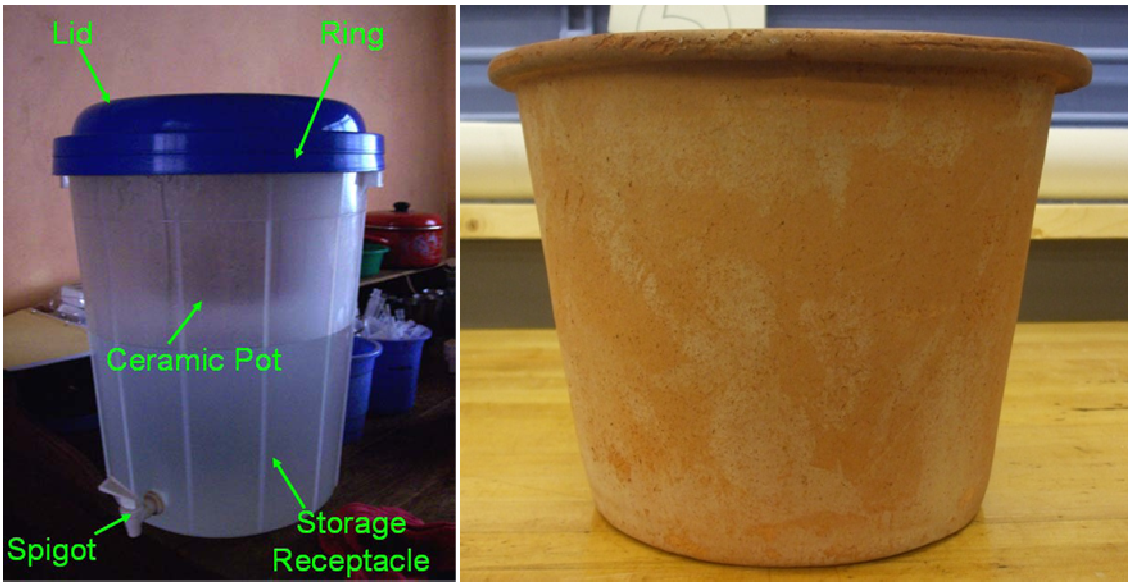

Figure 1-7: The *Kosim* Filter: Complete Unit at Left (PFP ctd. in Fitzpatrick, 2008); Ceramic Element at Right

The filter's lip rests on the plastic ring which fits snugly over the rim of the plastic storage receptacle. Water is poured into the CPF from above. The lid is then placed on top of the ring to prevent contaminants from entering the filter. The water then seeps through the CPF and into the food-grade plastic storage receptacle, where it can be decanted from the spigot.

1.2.3.3 Manufacture and Mechanisms of Filtration

In order to understand the mechanisms of filtration of the CPF, one must understand its composition and manufacture. Methods of manufacture differ from country to country, but the essentials remain the same. At the PHW factory in Ghana, which began producing its first filters in January, 2010, crushed clay is mixed with a burnout material (e.g., rice husk or sawdust), wedged into cubes, and pressed in a nylon mold using a hand-cranked portable PFP press. PHW also has the capability of producing filters using the press-and-mold designed and built by Emmanuel Hernandez, often referred to as the "Mani Press." After drying, the pots are loaded into a kiln and fired, at which time the burnout material combusts, leaving pores in the CPF. It is these pores which constitute the mechanical component of filtration.

The pores trap contaminants through the phenomena of mechanical screening, sedimentation, and adsorption (van Halem D. , 2006, p. 14).

1. Mechanical screening refers to the straining of particles which are too large to pass through the pore channels created by the burnout material (van Halem D. , 2006, p. 14). Potters for Peace has selected 1 μm as their desired pore diameter (Alethia Environmental, 2001a, p. 19).

2. Sedimentation refers to the deposition of particles on the interior walls of the filter (van Halem D. , 2006, p. 14)

3. Adsorption is the phenomenon wherein Van der Waals' forces, which arise from nuclear attraction between particles, and/or electrostatic attraction between opposing electrical charges, cause contaminants to adhere to the surface of the pore channels (van Halem D. , 2006, p. 14).

Once the filters have been fired and cooled, they are submerged in a solution containing colloidal silver. The colloidal silver coats the surface of the pore channels and chemically alters microbial and viral contaminants. The biocidal properties of silver have long been known, but their mechanisms of action have only come to light more recently. A few of the known biocidal interactions of silver are:

1. Removal of hydrogen atoms from thiol groups of bacteria and viruses. Thiol compounds are defined by their functional group, which contains a sulfur-hydrogen bond; once the hydrogen is stripped, sulfur atoms join one another and inhibit respiration;

2. Inhibition of DNA replication by interference with DNA unwinding;

3. Alteration of bacterial membranes via interaction with enzymic proteins

(Russell cited in van Halem 5; Niven 5).

1.2.3.4 Pure Home Water's Selection of the Kosim Filter

PHW chose the *Kosim* filter as its primary water treatment product for several reasons.

- The effectiveness of silver-impregnated CPFs has been well-documented. Studies have shown an *E. coli* removal efficiency of 97.8 to 100% in laboratory settings (Johnson, 2004, p. 3; Oyanedel-Craver and Smith quoted in Kallman et al., 2009, p. 21; UNICEF, 2007, p. 4).

- Use of the filters has been positively linked to a reduction in incidences of diarrhea. In Cambodia, for example, follow-up monitoring revealed that households using the filter reported only half the cases of diarrhea as compared with control houses not using the filter (UNICEF, 2007, p.4). In the Northern Region of Ghana specifically, Sophie Johnson found that people living in traditional households with filters had a 69% lower risk of diarrhea than people in households without the filters (2007, p. 3)

- The CPF can be manufactured almost entirely from local materials. All of the filter's elements are made in Ghana, with the exception of the imported spigots and colloidal silver solution (Fitzpatrick, 2008, p. 19).

- Water is already universally stored in large clay vessels in Northern Ghana, making the CPF a culturally acceptable technology (Murcott, 2009).

- Ghana's widely used surface water supplies are extremely turbid; CPFs are one of the few feasible technologies that can filter high-turbidity water. Figure 1-8 presents turbidity data, obtained using a turbidity tube, from selected dugouts in Northern Ghana. For purposes of comparison, WHO suggests a guideline value of approximately 0.1 Nephelometric Turbidity Units (NTUs) for effective disinfection (WHO, 2008, p. 219).

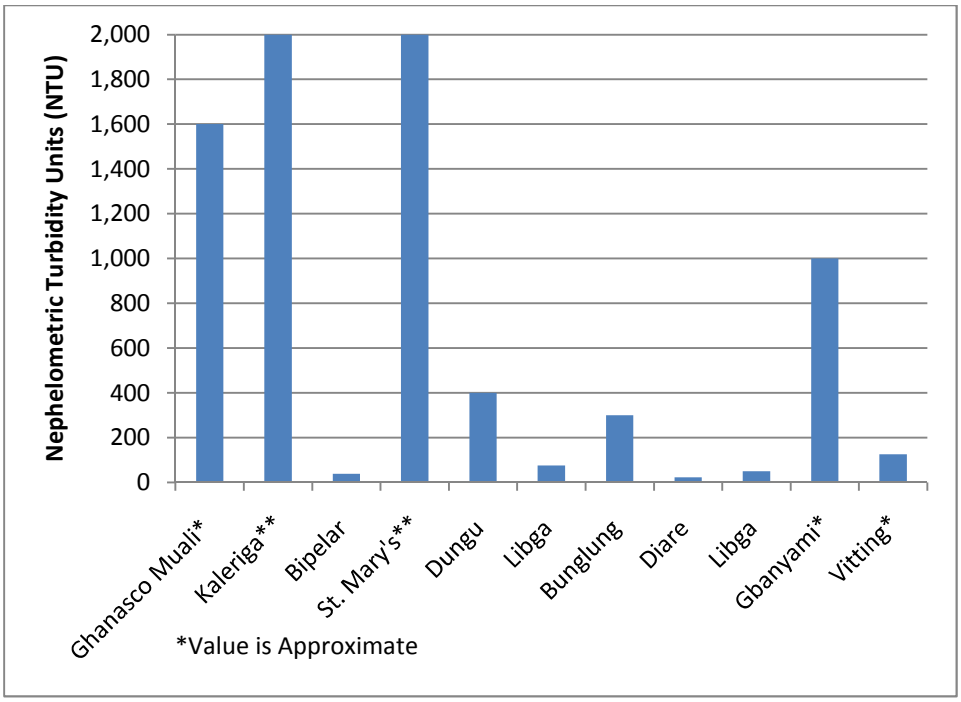

Figure 1-8: Turbidity in Selected Ghanaian Dugouts: (Adapted from Murcott, 2009)

1.3 Research Objectives

Though the Kosim filter has proven itself to be an appropriate, effective, and affordable method of water filtration in Ghana, it is not without its drawbacks. One complaint commonly lodged by users is that the filters are fragile. In some sense, this is unavoidable; the filters are effective precisely because they are highly porous – a feature which renders them subject to breakage. There are, however, parameters that may be altered within the limitations imposed by the necessity of the filter's porosity that may yield increases in the filter's durability.

The objective of this research is to determine the nature and extent of the effect of compositional and geometrical changes in the Kosim filter to its durability, specifically measured as bending strength. Recipes will be rank-ordered according to statistically significant comparative strength differences. This ranking will be included in a decision matrix along with rankings of flow rate and removal efficiency from a parallel study by Miller such that an optimum recipe may be selected. The desired outcome is a filter recipe and geometry which will produce filters with decreased rates of in-use breakage while maintaining acceptable pathogen removal efficiency and flow rate.

2 Previous Research On Breakage

Though an impressive volume of literature exists regarding the flow rate and pathogenic removal efficiency of CPFs (Bloem, van Halem, Sampson, Huoy, & Heijman, 2009; Alethia Environmental, 2001a; Leftwich, Yakub, Plappally, Soboyejo, & Soboyejo, 2009; Oyanedel-Craver & Smith, 2008), the literature on breakage of the filter is comparatively sparse. What literature exists focuses primarily on rates of breakage, rather than mechanisms or prevention of breakage. Even with this paucity of literature, however, the problem of breakage has proved ubiquitous.

2.1 Nicaragua

Concern for breakage of the filters first appears in Lantagne's field investigations in Nicaragua, published in 2001. Lantagne first mentions focus group meetings performed by students from Tulane University in 2000 in the communities of Ocotal, Matagalpa, and Malacotova. Students discovered a use rate of only 20% in Malacotova, which they partially attributed to leaking from the bronze spigots. The students recommended the establishment of a spare parts facility in each community for the replacement of broken filter elements (Alethia Environmental, 2001b, pp. 34-35).

In a separate field study performed by Lantagne, 33 homes were visited, spanning seven communities in three geographical locations of Nicaragua. Lantagne found that "Of the 33 houses visited, nine were not using the filter. The most common reason (6 homes) was that the filter or the filter and receptacle were broken" (Alethia Environmental, 2001b, p. 47). Lantagne implicitly identified the mechanism of impact as one cause of breakage, stating that homes in Mancotol used metal wire to secure their filters to the wall. Lantagne explicitly identified breakage around the lip of the filter and leakage around the filter's spigot as other causes for disuse, stating: "The most common problem seen was breakage of the filter, the receptacle, and the lip of the filter. In addition, leakage from the spigot was noted" (Alethia Environmental, 2001b, p. 55). Though breaking the lip does not always destroy the pot, it does create an avenue for untreated water to bypass the filter and contaminate the stored water, as well as causing possible cracks in the side of the filter for additional bypass (Desmyter, Adagwine, Ibrahim, Jackson, & Murcott, 2008, p. 17). Lantagne provides the following remedial recommendation: "Filters are ceramic, and as such break. Purchasing [an] extra filter at the beginning will allow for replacement of broken filters" (Alethia Environmental, 2001b, p. 56).

2.2 Cambodia

Following Lantagne's 2001 reports, UNICEF published a field note concerning the use of CPFs in Cambodia. In 2006, follow-up studies were performed on 506 randomly selected homes out of the 2000 households that had originally received the filters, some time between 0 and 44 months before initiation of the study (UNICEF, 2007, p. 3). Three-hundred fifty filters were found to be no longer in use; 328 households provided responses when asked why their filter was no longer in use. UNICEF found "A total of 214 (65%) were due to filter unit breakage, either of the ceramic filter element, the spigot, or the container" (UNICEF, 2007, p. 16). UNICEF continues: "[A] predicted 2% of filters may fall into disuse each month after implementation due primarily to breakage" (2007, p. 26), and mentions this to be consistent with a study performed in Bolivia by Clasen, et al., which found a 20% decline in use after nine months (UNICEF, 2007, p. 27). UNICEF's suggested remedy is the availability of replacement parts. To wit: "As units are subject to breakage over time, replacement parts and units are needed" (UNICEF, 2007, p. 34).

2.3 Research by van Halem

Breakage of the filter is also mentioned qualitatively in van Halem's extensive master's thesis from Delft University: Van Halem stated that, while the chances of breakage are minor for a filter remaining in its receptacle, "…[S]ince the lip is fragile and when handling the element this lip is used for carrying etc., breakage of the lip is usually the case after several cleaning sessions" (van Halem D. , 2006, p. 59). Furthermore, van Halem opined that the filter is more vulnerable when wet, which would of course be the case during cleaning (2006, p. 59). Finally, van Halem expressed concern as to cracks in the filter element, which, if unnoticed, may create an avenue for passage of pathogenic microorganisms (2006, p. 59). Van Halem recommends frequent, thorough inspections as an appropriate preventative measure (2006, p. 59).

2.4 Ghana

Most germane to the Ghanaian context is the 2007-2008 assessment by Desmyter, et al., in which follow-up evaluations were performed on 1,000 out of the 5,000 Northern Ghanaian households to receive the *Kosim* CPF in response to the September 2007 floods. Desmyter, et al.'s 2008 report found that, three to seven months after implementation:

- 12% of the filters were no longer in use because of a malfunctioning filter (p. 1);
- 95% of all breakage occurred in the household (p. 1);
- the weakest spot is the lip (p. 17);
- leakage occurs when the tap is incorrectly inserted in the perforation of the safe storage container (p. 17); and
- most CPF units malfunction because they are not properly handled, while marginally few malfunction due to fatigue failure (p. 18).

Figure 2-1 and Figure 2-2 provide photographs of broken Ghanaian filters.

Figure 2-1: Ghanaian Filter with Broken Lip (Murcott, 2009)

Figure 2-2: Ghanaian Filter with Presumed Impact Breakage (Murcott, 2009)

In light of their findings, Desmyter, et al. recommend prevention as the primary method of decreasing filter breakage: "The best approach for prevention is definitely to deliver a relevant and comprehensible education and practical training to the person who will control the ceramic filter unit" (2008, p. 18). The researchers do, however, mention that the filter may be made stronger by increasing its thickness from ½" (12.7 cm) to ¾" (19.1 cm) (2008, p. 19). Furthermore, Desmyter, et al. acknowledge that some breakage is inevitable, and suggest that repair services be made available so that households may resume use of their filters as quickly as possible (2008, p. 18).

Much of the literature discussed thus far focuses on remedial action that may be taken *after* breakage of the filter. Barbara Donachy, former US Coordinator for Potters for Peace, provided several suggestions for preventing the filter from breaking:

- thicken the lip, from ½" (12.7 cm) to ¾" (19.1 cm)
- provide a gasket between the ceramic filter and the storage container for prevention of failures that occur upon removing a stuck filter from an improperly sized storage container
- increase focus on quality control to guarantee adherence to existing guidance

(Barbara Donachy, personal communication, September 17, 2008)

3 Modeling the Filter

3.1 Potential Failure Mechanisms

As mentioned, very little research exists relating to the failure mechanisms of the CPFs. However, in a series of e-mails with Mary Kay Jackson, Managing Director of PHW in Ghana, three failure mechanisms were mentioned. Additionally, Section 2.4 mentions the identification of fatigue failure by Desmyter, et al (2008).

3.1.1 Impact Failure

In an e-mail from Mary Kay Jackson dated November 21, 2009, she mentions: "[W]e see impact failures due to either mishandling or more brittle clays." This confirms Lantagne's suggestion of impact breakage mentioned in Section 2.1. Thus, improving the impact strength of the filter may decrease the rate of breakage.

3.1.2 Shear Failure

In an e-mail dated November 22, 2009, Ms. Jackson wrote: "The lip failures generally seem to be shear failures early in the life of the pot," and "Pots are shipped in a stack of [three], and we would break pots just when pulling them apart." Desmyter et al. confirm that "Lip breakage usually happens when the ceramic pot is not gently handled or can occur when it is lifted out of the safe storage container while it is filled with water (2008, p. 17). Based on this testimony, investigation of shear strength may be informative for providing recommendations to prevent future breakage.

3.1.3 Bending Stress Failure

Ms. Jackson also wrote in her November 22, 2009 email that "…[I]t may be necessary to increase the lip's thickness as well to overcome the bending stress of lifting." As referenced in Section 2, Lantagne, Desmyter et al., and van Halem have all mentioned failure of the lip without specifying the mechanism of failure, but lifting the filter by its lip undoubtedly places both bending and shear stress on the filter, as will be shown in Section 3.2. Therefore, data from bending stress testing is of interest.

3.1.4 Fatigue Failure

Desmyter et al. mention that "[M]arginally few" filters fail due to fatigue (2008, p. 18). However, the failures described by Ms. Jackson all occur well before fatigue failure becomes an issue. It is therefore more critical to address impact, shear stress, and bending stress failure, which render filters useless or less effective soon after their manufacture.

3.1.5 Selection of Failure Mechanism for Investigation

Due to constraints of time, money, and equipment, not all potential failure mechanisms could be investigated within the scope of this thesis. Inferences were made in the hopes of selecting the failure mechanism whose investigation via material and geometric changes would be most likely to yield strength increases which could be realized with the resources currently available to PHW. Through conversations with Dr. Krystyn Van Vliet, MIT Associate Professor in the Materials Science Department of the Massachusetts Institute of Technology, and Dr. Tomasz Wierzbicki, MIT Professor of Applied Mechanics in the Department of Mechanical Engineering at the Massachusetts Institute of Technology, bending stress was determined to be the most promising mechanism of failure for investigation.

3.1.5.1 Dismissal of Investigation of Impact Failure

In addition to an investigation of bending stress failure, the American Society of Testing and Materials (ASTM) provides ASTM C368-88, Standard Test Method for Impact Resistance of Ceramic Tableware, which seems an appropriate method for investigating the impact strength of CPFs under their normal loading conditions. In this test, the rim and center of ceramic pieces are subjected to a schedule of impacts so as to determine the magnitude of the blow required to cause initial fracture and the amount of energy necessary to cause complete failure of the sample. Unfortunately, no apparatus meeting the specifications described in the standard was available. Although such an apparatus could have been manufactured, constraints of time and money forbade such an endeavor.

3.1.5.2 Dismissal of Investigation of Shear Failure

Tests for the shear strength of a material are difficult to design. ASTM does not provide a loading configuration that will place a ceramic material in pure shear, i.e., shear force without moment force. Furthermore, Dr. Wierzbicki suggested that the performance of a bending-stress test would be sufficient for rank-ordering the strength of the material, and further testing on impact and shear failures would neither affect the rank-ordering nor provide useful additional information (personal communication, December 2009). Thus, investigation of shear failure was not pursued.

3.1.5.3 Investigation of Bending Stress Failure

As mentioned, bending stress failure was determined to be the most promising mechanism for investigation. The author patterned the selected test method after ASTM C674-88, Standard Test Method for Flexural Properties of Ceramic Whitewares.[5] The details of the employed test method are presented in Section 4.5

3.2 Modeling Stresses in the Lip of the Ceramic Pot Filter

3.2.1 Measurement of Dimensions

In order to model the bending stress in the lip, one must obtain dimensions of the CPF. Investigations on a fractured pot from the PHW factory in Tamale, Ghana, are included in Figure 3-1 and Table 3-1. The methods of measurement are detailed in APPENDIX A.

The measurements with asterisks were obtained from AutoCAD 2010© rather than from direct measure. In fact, if only measurements obtained from direct measure had been used, a symmetrical, geometrically consistent pot could not be produced, due to the variation in the measurements and the warping of the pot. Thus, a set of minimum requisite measurements was employed.

It should be noted that PHW also has the capability of producing a paraboloid-shaped filter from the aforementioned Mani Press. The author has not recorded dimensions of or modeled forces on the paraboloid filter. However, the rank-ordering of material compositions based on bending strength and the bending strength gained from geometrical variations in the lip will apply to filters of any shape. Statements about the expected stresses experienced by the lip, however, apply only to the flower-pot shaped filter.

[5] "Whiteware" refers to a broad class of ceramic products, including earthenware such as the CPF (Whiteware, 2010).

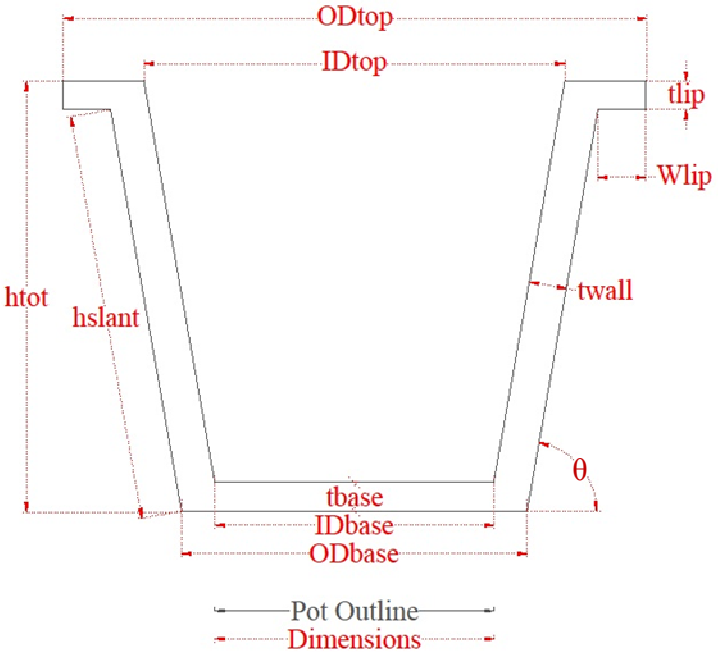

Figure 3-1: Diagram of the PHW Filter from Tamale, Ghana

Table 3-1: Measurements of the PHW Filter from Tamale, Ghana

Dimension	Measurement
OD_{top}*	30.7cm
ID_{top}*	22.2cm
OD_{base}	18.2cm
ID_{base}	14.7cm
t_{lip}	1.5cm
t_{wall}*	2.0cm
t_{base}	1.5cm
h_{tot}*	22.7cm
h_{slant}	21.5cm
W_{lip}	2.5cm
θ	80°

**Obtained from AutoCAD 2010©*

Van Halem has provided a similar set of measurements for the Ceramica Tamakloe Ltd. filter, a Cambodian filter, and a Nicaraguan filter (2006). These measurements have been adapted and included in APPENDIX B.

3.2.2 Modeling of Loading Condition

Now, one wishes to model the forces experienced by a filter when lifted by its lip. First, consider a rendering of the CPF carrying its full capacity of water in Figure 3-2 below.

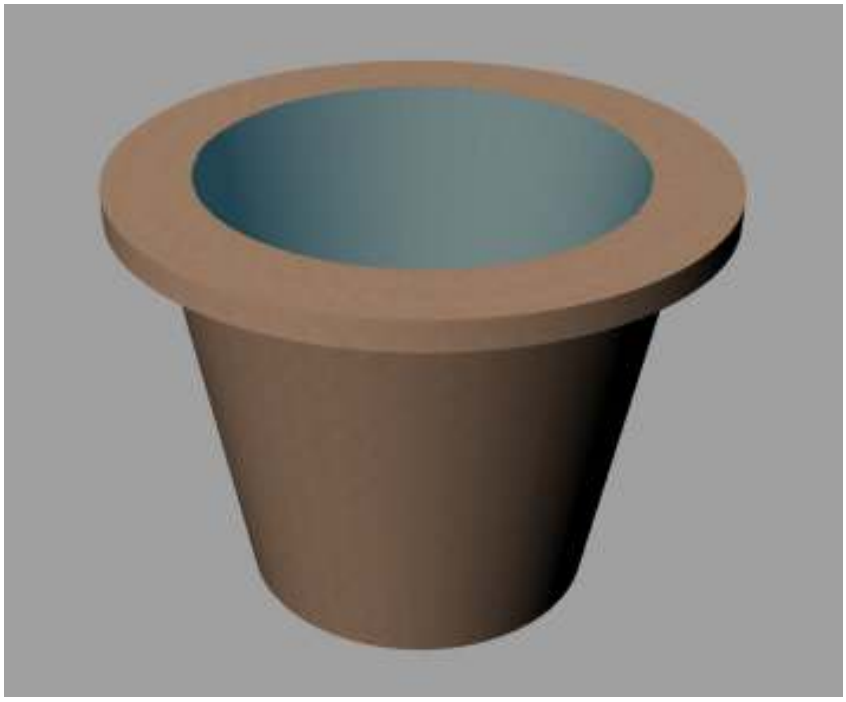

Figure 3-2: Rendering of Pot with Full Water Load

Now consider an infinitesimally thin cross-section of the filter. We may quantify the weight forces acting on this cross-section per unit length and unit depth by considering the density of the pot, the density of water, and the vertical extent of each substance at each position on a horizontal *x*-axis. The scenario is depicted in Figure 3-3.

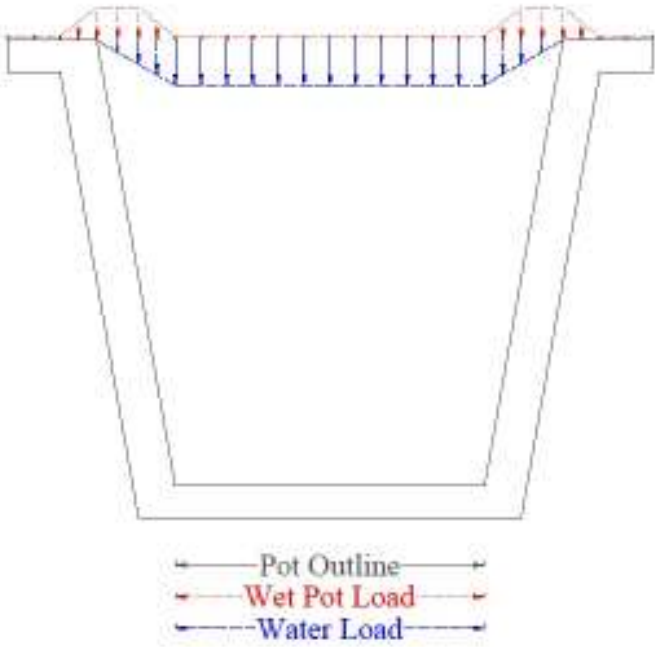

Figure 3-3: Loading Condition of Ceramic Pot Filter

Two separate loads are represented:

1. the load due to the wet pot, and
2. the load due to the contained water.

Notice that the wet pot load changes as one traverses the filter wall; this is due to the fact that a vertical line through the pot intersects first an increasing portion of the filter's wall, then a constant portion, then a decreasing portion until only the base is intersected. Similar arguments apply for the water load. The arrows representing the load forces have been scaled such that their relative lengths represent the relative magnitudes of the loads.

Forces located at any radius *r* from the center of the filter are equal. Thus, the sum of the moments about any axis that is perpendicular to the direction of the application of the forces and that intersects the filter's center is zero. We may then resolve the forces into two weight loads, equal to the sum of the weight loads contributed by the pot and its contained water, acting perpendicular to the plane of the filter's base and through the center of the filter's base. The situation is depicted in Figure 3-4.

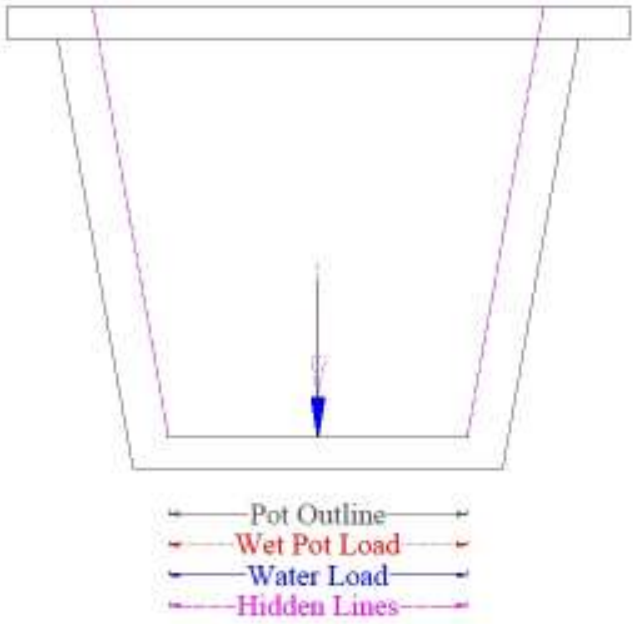

Figure 3-4: Resultant Weight Forces Acting on the Ceramic Pot Filter

Hidden lines have been added to emphasize that one is now looking at an elevation view of the pot, not an infinitesimal cross-section – the resultants include the contribution from the entire wet pot load and the entire water load, not the contribution from an infinitesimally thin cross-section alone.

One wishes to determine the magnitude of these loads. Now, it is well known that $W=\rho g V$, where ρ is density, g is the acceleration due to gravity, and V is volume. The volume of the pot and its contained water were obtained from AutoCAD 2010© and geometry, respectively. The density of water is well-known for given temperatures; one will assume room temperature (25° C) for this calculation. The dry density of each pot was obtained by averaging the mass of 26 CPFs produced at the PHW factory in Tamale, Ghana and dividing by the volume obtained from AutoCAD 2010©. The wet density is related to the dry density by:

$$\rho_{wet} = \frac{M_{Pot,Wet}}{V} = \frac{n(V)(\rho_{water}) + M_{Pot,Dry}}{V},$$

Equation 3-1

where n is the porosity of the pot. One may adapt an average porosity of 0.38 from the measurements of Van Halem (2006, p. 17).

The weights and associated parameters are presented in Table 3-2.

Table 3-2: Density, Volume, and Weight of Wet Ceramic Pot Filter and Contained Water

	Wet Pot	Water
ρ	1.35g/cm^3	1.00g/cm^3
V	3,500cm^3	5,700cm^3
W	46 N	56 N

When supporting the pot with one's hands, the entire weight of the pot and the contained water must be countered by the hands' upward force. This force is modeled as a linearly decreasing distributed load, seen in the closeup of the filter's lip, Figure 3-5.

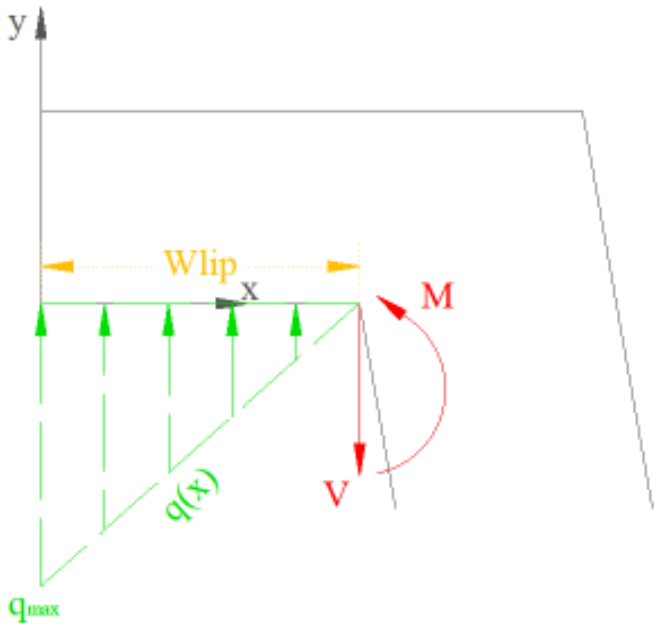

Figure 3-5: Closeup of Filter Lip

Notice that the intersection of the filter lip with the filter wall is modeled as a fixed support, with shear reaction force *V* and moment reaction force *M*. The arrows representing the magnitude of the hand load, shear reaction force, and moment reaction force are not to scale. The distributed load representing the self-weight of the wet pot has been neglected; this is a conservative assumption, as it creates a larger moment, and is a reasonable simplification, given that the self-weight of the lip is small compared to the hand load.

The choice of the linearly decreasing load as a model for the upward force provided by a lifting hand is predicated on the idea that a person lifting the filter will exert more force on the outer edge of the lip than on the inner edge. Furthermore, this loading is conservative in that it creates a greater moment force than either a uniform or linearly increasing load, since the majority of the force is concentrated *away* from the fixed support.

For simplicity of calculation, we may resolve the distributed load into its resultant force, which maintains the condition of equilibrium without changing the value of the moment at the fixed support. The resultant of a distributed load acts through the centroid of the area of the distribution, which, for a triangle, is located at two-thirds of its height. For the orientation presented in Figure 3-5, the resultant acts at location $x = W_{lip}/3$, as depicted in Figure 3-6

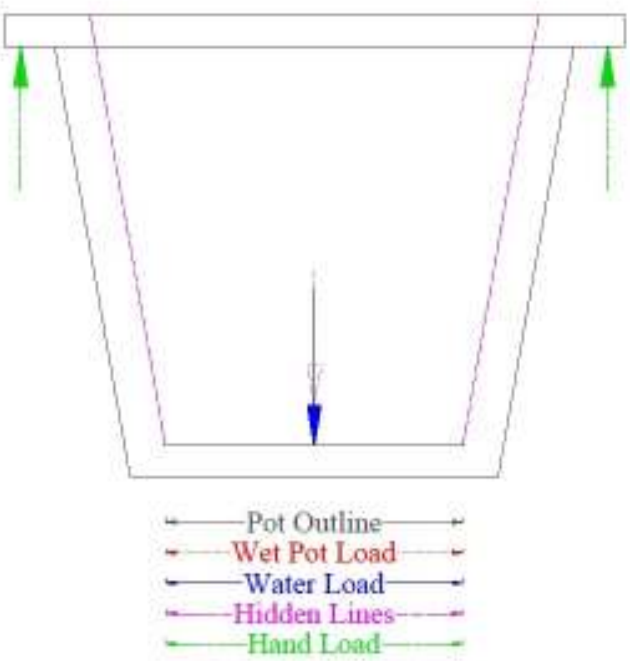

Figure 3-6: Resultant Forces Acting on Ceramic Pot Filter in Equilibrium

Because the resultant hand load must balance the resultant weight loads from Figure 3-4, one writes:

$$\sum F \downarrow + = \left(W_{WetPot} + W_{Water}\right) - 2H = 0 \ ,$$

Equation 3-2

where H is the resultant force of the hand load. This may be rearranged as follows:

$$H = \frac{W_{WetPot} + W_{Water}}{2}$$

Equation 3-3

From the values listed in Table 3-2, one finds H = 51 N, and all resultant values of the loading condition have been determined.

3.2.3 Calculation of the Maximum Bending Stress

Modeling the forces as a linearly decreasing distributed load allows one to determine a function for the maximum moment experienced by the lip of the filter, which occurs at the fixed support:

$$M_{max} = \frac{q_{max} W_{lip}^{\ 2}}{3}$$

Equation 3-4

This result is derived in APPENDIX C.

Now, H is equivalent to the area under the curve of the distributed load, which, for the triangle, may be written:

$$A = H = \frac{q_{max} W_{lip}}{2}.$$

Equation 3-5

One may rearrange this equation as follows:

$$q_{max} = \frac{2H}{W_{lip}}.$$

Equation 3-6

Substituting Equation 3-6 in Equation 3-4 yields:

$$M_{max} = \frac{2H}{W_{lip}} \frac{\left(W_{lip}\right)^2}{3} = \frac{2}{3} H W_{lip}.$$

Equation 3-7

Substituting Equation 3-3 for H in Equation 3-7 yields:

$$M_{max} = \frac{2}{3} \frac{\left(W_{WetPot} + W_{Water}\right)}{2} W_{lip} = \left(\frac{W_{WetPot} + W_{Water}}{3} \right) W_{lip}.$$

Equation 3-8

The hand will act over a portion of the filter's circumference. Continuing to model this portion of the filter as a cantilevered beam, one may assign the beam a dimension, c, equal to the portion of the filter's circumference over which the hand acts. The extent of this dimension will be equal to the width of the four fingers used in lifting the pot; this width has been taken as equal to the width of the author's four fingers, which is approximately 5cm. The beam is depicted in Figure 3-7.

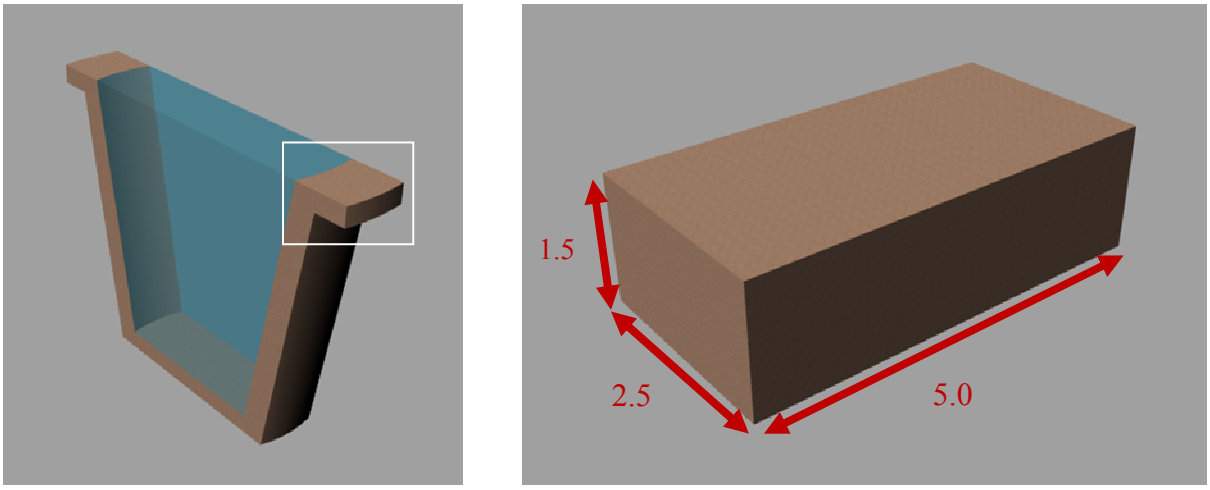

Figure 3-7: Extracted Cantilever Beam From Lip of Ceramic Pot Filter (dimensions in cm)

A further assumption has been made in considering a rectangular beam to be a good approximation to a beam arising from the filter's true geometry.

The testing procedure will yield data as to the modulus of rupture of the various materials. The modulus of rupture is a material property which describes the greatest bending stress that a material can withstand under bending before it ruptures. Moment and bending stress in beams are related according to the following equation:

$$\sigma = \frac{-My_c}{I_{x'}},$$

Equation 3-9

where:

σ is the stress at y_c

M is the applied moment

y_c is the distance from the y-coordinate of the beam's centroid to the position at which σ is considered, and

$I_{x'}$ is the moment of inertia of the cross-section about its centroidal x-axis.

The negative is a sign convention indicating that the beam experiences:

- compressive stress, considered negative, at locations above the centroid, where y_c is positive, and
- tensile stress, considered positive, at locations below the centroid, where y_c is negative.

In this analysis, one is concerned primarily with the magnitude of the stress; thus the negative sign will be removed in subsequent equations.

For a rectangular cross-section, the y-coordinate of the centroid is located at the midpoint of the cross-section. For purposes of this analysis, one will concern oneself with the maximum moment, which occurs when y_c is greatest, i.e., at the outermost fiber of the beam. At this location, y_c equals one-half the thickness, t, of the cross-section. That is:

$$y_c = \frac{t}{2},$$

Equation 3-10

The moment of inertia about the horizontal centroidal axis, x', is:

$$I_{x'} = \frac{1}{12} w t^3,$$

Equation 3-11

where w is the width of the cross-section. In subsequent equations, w will be replaced with c, the portion of the filter's circumference over which a lifting hand acts.

Substituting Equation 3-10 and Equation 3-11 in Equation 3-9 yields:

$$\sigma_{max} = \frac{M\frac{t}{2}}{\frac{1}{12}ct^3} = \frac{6M}{ct^2},$$

Equation 3-12

where the subscript *max* indicates that one is considering the maximum value of compressive stress by choosing the maximum value of y_c.

One may replace M in Equation 3-12 with $M_{\max}$ from Equation 3-8 to determine a formula for the maximum bending stress expected in the lip of the CPF.

$$\sigma_{max} = \frac{6\left(\frac{W_{WetPot} + W_{Water}}{3} W_{lip}\right)}{ct^2} = \frac{2\left(W_{WetPot} + W_{Water}\right)}{ct^2} W_{lip}$$

Equation 3-13

Replacing now all of the variables in Equation 3-13 with the known values from Table 3-1 and Table 3-2, and letting c = the approximate width of the fingers used to lift the pot (5cm), one may obtain the maximum bending stress that the lip of a full filter must endure as:

$$\sigma_{max,full} = 0.45MPa$$

Equation 3-14

If this value exceeds the modulus of rupture, *R*, calculated from the test procedure described in Section 0, one predicts that a filter manufactured in the same conditions as the test sample will break if lifted while carrying a full load of water.

If one omits the water weight, one may obtain the maximum stress endured by the lip of the filter while carrying only its wet self-weight:

$$\sigma_{max,empty} = 0.20MPa$$

Equation 3-15

If this value exceeds the modulus of rupture, *R*, calculated from the test procedure described in Section 0, one predicts that a wet filter manufactured in the same conditions as the test sample will break if lifted while empty.

3.2.4 Calculation of the Maximum Shear Stress

It is now a trivial matter to calculate the maximum shear stress experienced by the filter. Shear stress is defined as:

$$\sigma_v = \frac{P}{A},$$

Equation 3-16

where P is the load acting parallel to a plane of cross-sectional area A. For the beam of Figure 3-7:

$$\sigma_v = \frac{H}{ct}.$$

Equation 3-17

Using the known values, one finds σ_v = 0.068 MPa for a CPF bearing a full water load and σ_v = 0.031 MPa for an empty CPF. The implications of the presence of shear stress will be discussed in Section 3.3.

3.2.5 Summary of Key Results

Table 3-3 provides a summary of the key results from Section 3.2.

Table 3-3: Summary of Key Results for Stresses in the Lip of the CPF

	Wet CPF, Full Water Load	Wet CPF, Empty
Maximum Expected Bending Stress	0.45 MPa	0.20 MPa
Maximum Expected Shear Stress	0.068 MPa	0.031 MPa

3.3 Limitations to Modeling and Testing Methods

3.3.1 Neglected Shear Forces

In truth, the situation depicted in Figure 3-3 through Figure 3-5 is a simplification of the loading condition. The beam has been created by removing a portion of the pot and applying the calculated loads. However, the removed portion of the filter would exert shear forces on the faces exposed by its removal. Figure 3-8 depicts a thin slice of the filter including the shear forces exerted by the filter's removed portion.

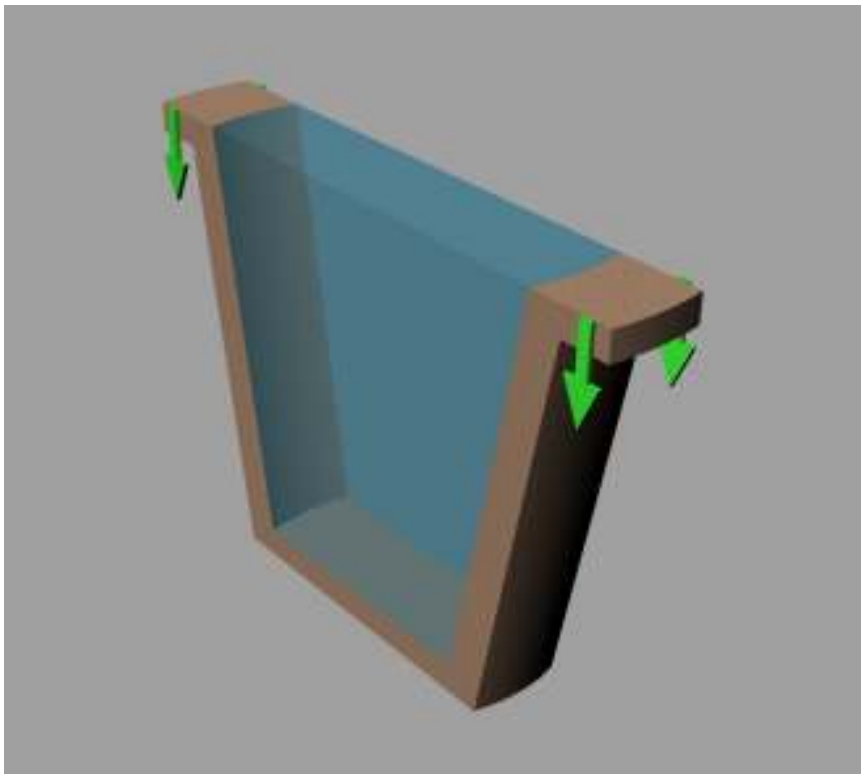

Figure 3-8: Rendered Strip of Pot With Shear Forces

This force has been neglected in the analysis; to consider it would result in a statically indeterminate condition, i.e., a condition which results in a system of n linear equations with m unknowns, where $m > n$. Proper characterization of this condition requires numerical analysis methods, in which algorithms utilizing numerical values are applied to develop an approximate solution to a continuous problem in lieu of an exact analytical solution. One method of numerical analysis often applied to structural analysis problems is the Finite Element Method, in which a continuous member is divided into elements whose characterization generates a deterimnate system of simultaneous equations which may then be solved to describe the stresses at any point in the member with reasonable accuracy (Cook, Malkus, & Plesha, 1989, p. 2). The development, calibration, and application of such a model is time-consuming, and such a method is beyond the scope of this research. Under the advice of Professor Van Vliet, the previously discussed simplifications were deemed to describe a reasonable approximation to the true loading condition, and were therefore employed.

3.3.2 Neglected Interaction of the Shear and Bending Forces

Dr. Wierzbicki and Dr. Connor, Professor in the Department of Civil and Environmental Engineering, have stated that shear and bending work in tandem to create failure (personal communication, December 2009). That is, a material subjected to a shear stress of magnitude x_1 will fail under a bending stress of magnitude x_2, while a material subjected to a shear stress of magnitude $y_1 \neq x_1$ will fail under a bending stress of magnitude y_2 not necessarily equal to x_2. The inclusion of shear stress creates an additional tensile stress on a beam element. This tensile stress is maximized on the plane angled forty-five degrees from the direction of application of the force. This tension acts in tandem with the tension created via the moment force. The interaction of the tensile stresses arising from shear and bending creates a failure envelope detailing the combined shear and bending loads that a material can withstand; points outside of the envelope imply failure. Such an envelope is depicted schematically in Figure 3-9.

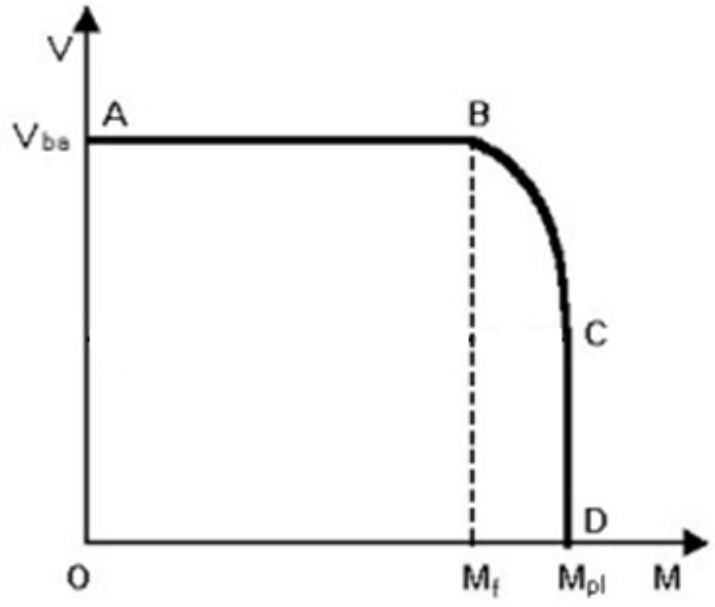

Figure 3-9 (Adapted from University of Ljubljana)

The bending stress test described in Section 0 is intended to place the material into nearly pure bending, i.e., into a condition in which the shear stress is too small to influence the magnitude of the bending stress at which the material will fail. That is, it attempts to place the material into a loading condition represented by the portion of the curve labeled CD, where M_{pl} is the maximum bending stress that the material may withstand even when the shear load is zero. One says that bending is the primary failure mechanism in this condition.

It is possible that the actual bending stress which may be withstood by the lip of the filter is less than this value obtained from testing because that the lip is subjected to both shear and bending. That is, it is possible that the actual loading condition experienced by the filter is not described by the region CD on the graph, but rather by the region BC, in which shear influences the allowable moment, or even AB, in which shear is the dominant failure mechanism. This possibility will be revisited in Section 5.3.1.2.

Proper development of this shear-moment interaction diagram is difficult, and involves fixing the bending stress while varying the shear stress, or vice-versa. Moreover, such a test would require more samples than could be feasibly manufactured, transported, and tested for this thesis. Furthermore, because the major desired outcome of this research is a rank-ordering of the material compositions in terms of strength, and because bending strength gains/losses often accompany shear strength gains/losses, determination of *whether* the material will fail under ordinary loading, and by what mechanism, is of secondary concern. Dr. Wierzbicki suggested that a single configuration of the bending stress test, and a rank ordering based upon such a test, was a reasonable substitute for the full development of this curve (personal communication, December 2009).

4 Methodology

Sections 4.1 through 4.4 describe actions taken while in the field in Tamale, Ghana in order to produce samples representative of actual field conditions. These samples were then transported in carry-on luggage to MIT so as to carry out the testing described in Section 4.5, which required equipment not available in Ghana.

4.1 Method of Material Preparation

The author produced a total of 150 clay beams of unfired length 115 mm, unfired width 25 mm, and unfired thicknesses of either 15 mm, 20 mm, or 25 mm. All raw materials were obtained from local sources in Ghana's Northern Region. They included:

- Clay taken from a pit in the town of Gbalhi;
- Grog[6] produced from broken PHW pots, manufactured earlier by Ceramica Tamakloe, Ltd.;
- Rice husk obtained from local farmers;
- Sawdust obtained from local mills; and
- Water obtained from a dugout in the town of Taha.

The material preparation process for the clay was as follows:

1. Break clay clods into small (< 5 cm diameter) pieces by hand or by hand tools.
2. Spread clay pieces on a tarp and let dry in sun for 1 to 2 days under sunny sky conditions. Samples are sufficiently dry when, if broken apart, they show no color change in their centers due to remaining moisture.
3. Pound clay to a fine powder using mortar and pestle.
4. Pour the clay powder through a 1 mm by 2 mm mesh.

Figure 4-1 illustrates the steps in this process

[6] grog refers to previously fired ceramic material that has been crushed to a desired particle size.

Breaking & Drying Clay | Pounding Clay | Sieving Clay

Figure 4-1: Steps in the Method of Clay Preparation (Photo Credit: Murcott [Far Left], Leah Nation [Center and Right], 2010)

The material preparation process for the sawdust and rice husk was as follows:

1. Place the combustible material into a 2-horsepower-engine hammermill of the kind shown in Figure 4-2.

Figure 4-2: Hammermill (Closed at Left, Photo Credit: Leah Nation, 2010; Open at Right)

2. Allow material to mill for a period of approximately one minute.
3. Collect milled material from both the waste chute, located at the bottom of the hammermill, and the radial chute.
4. If desired, sieve the remaining materials through a 1 mm by 2 mm mesh. This step was performed only for recipes #13 and #14.

4.2 Method of Mixing

Materials were hand-mixed by local potters. The recipes for each of the 14 mixes are shown in Table 4-1 below. The water content of each mixture was determined by the expert judgment of local potters, and varied for each pot produced. The water is added solely for the purpose of increasing malleability of the mixture, and is removed during the drying and firing processes. Therefore, it does not have any expected effect on the filtering ability, flow rate, or strength properties of the resultant filter.

Table 4-1: Filter Recipes (Adapted from Miller, 2010)

ID	Combustible Type	Hammermill Product	Grog Added?	Clay Mass (kg)	Grog Mass (kg)	Combustible Mass (kg)	Fine Combustible Mass (kg)	Waste Combustible Mass (kg)	Total Mix Mass (kg)
1	Rice Husk	Fine and Waste	No	11	0	3.00	1.50	1.50	14.00
2	Rice Husk	Fine and Waste	Yes	11	1	3.00	1.50	1.50	15.00
3	Rice Husk	Fine and Waste	No	11	0	4.00	2.00	2.00	15.00
4	Rice Husk	Fine and Waste	Yes	11	1	4.00	2.00	2.00	16.00
5	Rice Husk	Fine and Waste	No	11	0	5.00	2.50	2.50	16.00
6	Rice Husk	Fine and Waste	Yes	11	1	5.00	2.50	2.50	17.00
7	Sawdust	Fine and Waste	No	11	0	2.19	1.09	1.09	13.19
8	Sawdust	Fine and Waste	Yes	11	1	2.19	1.09	1.09	14.19
9	Sawdust	Fine and Waste	No	11	0	2.91	1.46	1.46	13.91
10	Sawdust	Fine and Waste	Yes	11	1	2.91	1.46	1.46	14.91
11	Sawdust	Fine and Waste	No	11	0	3.64	1.82	1.82	14.64
12	Sawdust	Fine and Waste	Yes	11	1	3.64	1.82	1.82	15.64
13	Sawdust	Fine Sieved	No	11	0	1.82	1.82	0.00	12.82
14	Rice Husk	Fine Sieved	No	11	0	2.55	2.55	0.00	13.55

4.3 Method of Casting and Drying Samples

After mixing, the samples eventually used in the bending stress tests were cast using the three molds shown in Figure 4-3.

Figure 4-3: Molds For Casting Samples

Each mold has dimensions of 115 mm in length and 25 mm in width, with thicknesses of 13 mm, 20 mm, and 25 mm.

The procedure for casting and drying was as follows:

1. Begin with clean wood block, wood mold, butter knife, and Sparco™ Brand stamper. Also begin with moist clay of one of the 14 mixtures shown in Table 4-1.
2. Press clay into mold from either side, flattening with palms.
3. Use flat edge of butter knife, with fingers pressed down on either side, to screed off the excess from one side.
4. Clean the knife
5. Repeat step 3 for the other side of the mold.
6. Place the mold on a flat surface and use a wet finger to smooth the clay surface. Fill in patches if necessary by adding a dab of clay to the moist finger.
7. Flip over the mold and repeat step 6 for the other side.
8. Stamp one side of the clay.
9. Using the wood block extruder, hold the mold in the air with two hands and use thumbs to apply pressure to the unstamped side of the clay until the clay is free from the mold.

10. Using a wet finger, smooth the newly exposed surfaces of the clay. Fill in patches if necessary by adding a dab of clay to the moist finger.
11. Gently pry the clay from the extruder with fingers by loosening the clay along the extruder's length.
12. Place sample stamp-side-up on a flat surface.
13. Continue until 10 samples of one recipe type are prepared.
14. Place a flat board over the samples and leave them in the shade to dry for approximately 24 hours.
15. After 24 hours, move the samples into the sun to dry. Rotate the samples 90 degrees counterclockwise about their longitudinal axis once every 30 minutes. Continue for approximately eight hours.
16. Replace the samples, uncovered, in the shade.
17. Repeat steps 15-16 until samples are dry on all sides.
18. Leave samples in the shade, uncovered, until they can be fired in the kiln.
19. Repeat all steps until 10 samples of each of the 14 recipes and 10 samples of the 13 mm-thick and 25 mm-thick versions of recipe #4 have been prepared.

Figure 4-4 provides photographs of the important steps in the process along with the corresponding step number.

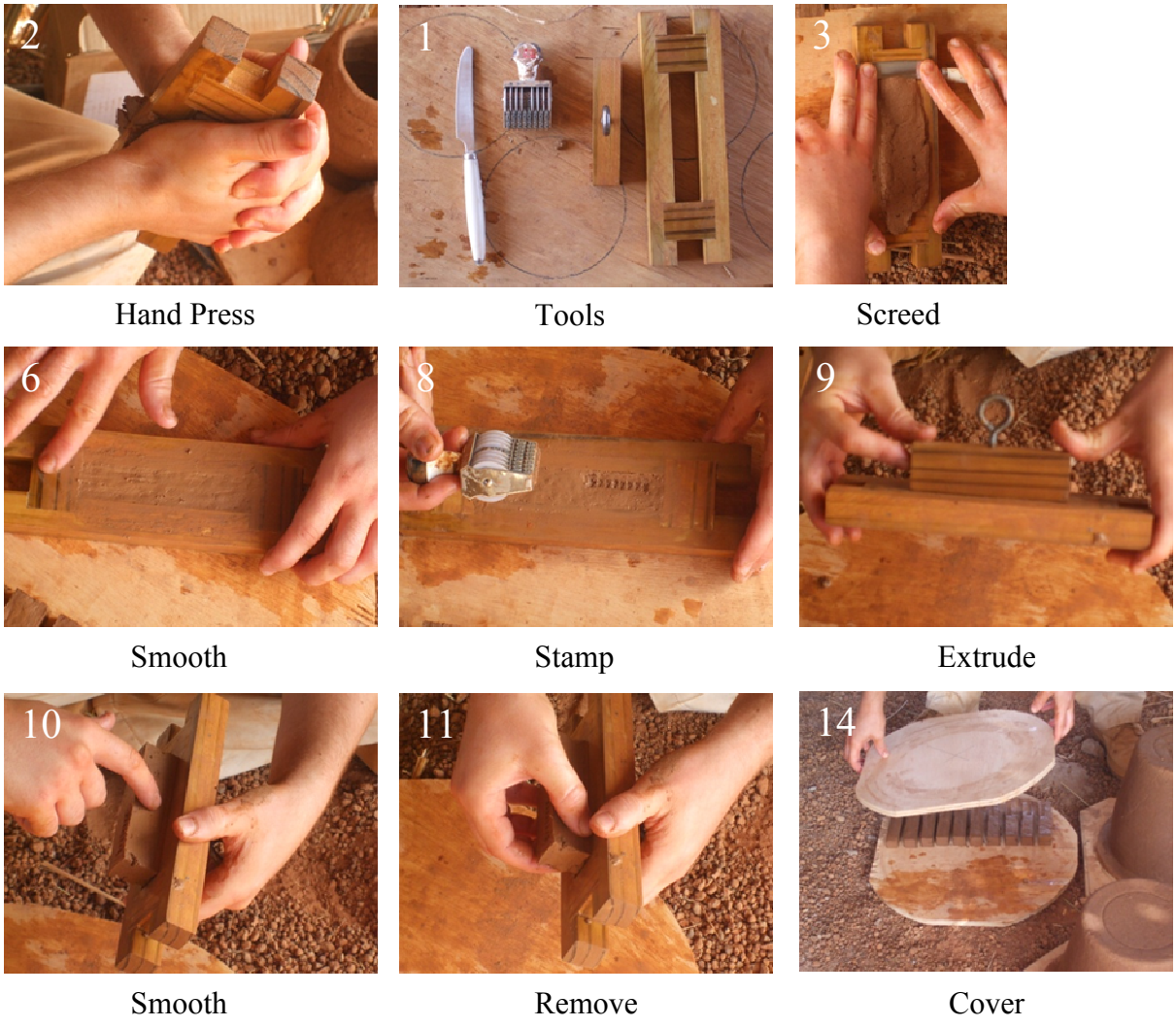

Figure 4-4: Key Steps in the Method of Casting and Drying Samples (Photo Credit: Leah Nation, 2010)

4.4 Method of Firing

The samples were fired in the downdraft brick kiln, designed and built by Emmanuel Hernandez and known as the Mani kiln, shown in Figure 4-5 and Figure 4-6

Figure 4-5: Downdraft Mani Kiln, Showing Mortar-Sealed Door (Photo Credit: Leah Nation, 2010)

Figure 4-6: Downdraft Mani Kiln, Showing Fireboxes

The samples were loaded into the kiln as shown by photograph in Figure 4-7 and schematically in Figure 4-8.

Figure 4-7: Loading of Clay Beams

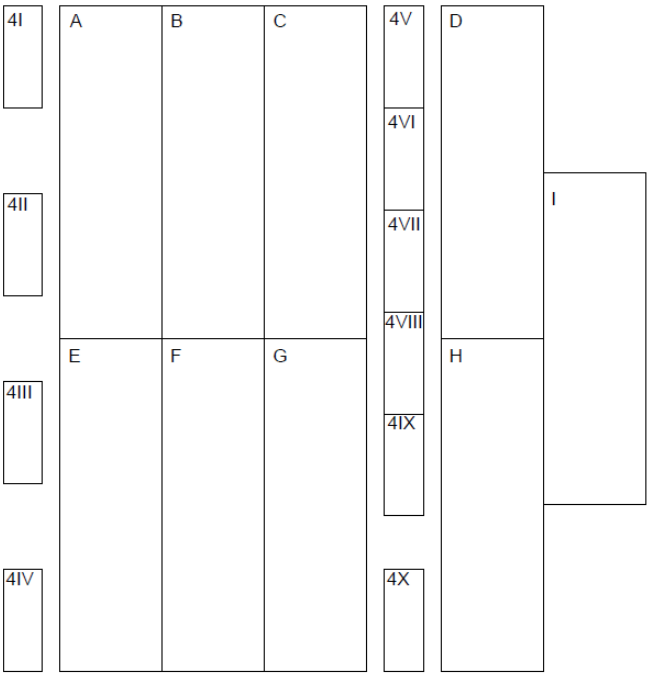

Figure 4-8: Schematic of Kiln Loading

In the schematic, a plan view of the kiln is divided into rectangular regions. The samples loaded into each rectangular region of the kiln were labeled with the name assigned to that region, such that the position that a particular sample had occupied within the kiln would be known. In each of the rectangular regions labelled A through I, one sample of each of the fourteen recipes was placed. That is, region A contained one sample each of recipes #1, #2, #3…#14. All of these samples had a uniform thickness before firing of 25 mm. In each section designated by Roman numeral, the author placed one sample of thickness 13 mm and one sample of thickness 20 mm. Recipe #4 was used for these samples; as such, each of these smaller rectangular regions is designated by the number 4, followed by a Roman numeral denoting the samples' positions.

4.5 Method of Breaking Samples

4.5.1 Equipment

The three-point bending test employed in the breaking of samples required a significant amount of equipment, provided by the MIT Civil and Environmental Engineering Laboratory. A list of the major equipment used is provided in Table 4-2.

Table 4-2: Equipment List for Three-Point Bending Test

Item Name	Model #	Serial #	Catalogue #	Additional Information
Instron Frame Model 1331	A488-109	8031-175	---	---
Instron 3-Point Support Apparatus	---	---	T112-1029	---
Interior 3-Point Supports	---	---	T1122-1040	---
Instron Load Cell 1	---	UK008	2518-011	Calibrated by: Beau Mooney, American Calibration, 12/11/08. Range: 200kNS, 100kND*, T & C°
Instron Load Cell 2	---	UK 009	2518-602	Calibrated by: Beau Mooney, American Calibration, 12/11/08. Range: 20kNS, 10kND*, T & C°
Instron Extensometer	---	2620-601	---	Range: ±5 mm
Instron Interface	8520 FIB	---	---	---
Instron Power Supply	8500 Tower	---	C2140	---
Instron Hydraulic Pump	A440-32	575	---	---
Instron Console: Linear 8500	8500 Panel	C2140	---	---
Data Collector: IOTech Personal Daq/56	---	262046	---	---
Software: Acqlipse 3302.018b	---	---	---	Created by Stephen Rudolph, Nov. 21, 2007
Hardware: Dell Optiplex GX 110	MMP	32T1NO1	---	---

**S and D designate Static and Dynamic loading, respectively*
°T and C designate Tension and Compression, respectively

4.5.2 Experimental Procedure

The experimental procedure described here closely mimics that prescribed by ASTM C 674: Standard Test Methods for Flexural Properties of Ceramic Whiteware Materials. Some important deviations include:

- Samples were not cooled in a dessicator, nor were they incubated in an electric oven at 110° C, as prescribed by the standard. The lack of equipment in Ghana, where the beams were produced, and the necessity of transporting the samples from Ghana to MIT in Cambridge, MA, precluded adherence to these guidelines.

- Samples were tested wet, as opposed to dry, due to the desire to recreate in-use conditions.

- The thickness of the specimen was varied, so as to determine the corresponding change in bending strength. Furthermore, the thickest (and presumably strongest) of the three variations (25 mm) was used when varying the compositional recipes so as to prevent breakage of the samples during transport from Ghana to MIT. This is in contrast to the ASTM-recommended 12.7 mm thickness.

- All dimensions – length, width, and thickness – deviate slightly from those prescribed by the standard. Though the samples were cast at the prescribed length and width dimensions, shrinkage of the clay during drying and firing reduced the dimensions.

- One-inch-diameter rollers were used for the supports and the load applicator, as opposed to knife edges rounded to 1/8" (3.2 cm) radii; these knife edges were unavailable.

- The test was performed under deformation control, as opposed to the prescribed load-control. Load-control tests carry a larger tendency to damage equipment, being that stresses build up in the material and release suddenly upon breakage. Furthermore, if the operator is not attending the machine closely, the actuator will punch through the material and continue to accelerate until it meets another resisting force to match its current loading level. Under the direction of Stephen Rudolph, lab supervisor in MIT's Department of Civil and Environmental Engineering, a deformation-controlled test was deemed appropriate.

Tests were carried out under the supervision of Stephen Rudolph. The resulting test method was as follows:

1. Obtain dry, fired samples approximately 22 mm by 22 mm by 105 mm, labeled on one of the 22 mm by 105 mm faces. For the samples with varied thicknesses, dimensions should be approximately 22 mm by 13 mm by 105 mm and 22 mm by 25 mm by 105 mm.

2. Soak samples for a period of no less than 24 hours, in accordance with Van Halem's recommended soak time required to obtain a constant water flux through the porous ceramic material (van Halem D. , 2006, p. 32).

3. Remove one sample from the soaked samples and pat dry on all sides.

4. Sand the two 22 mm by 105 mm faces of the sample which are orthogonal to the labeled face.

5. Measure and record the thickness (the dimension parallel to the direction of application of force) and width (the shortest dimension perpendicular to the direction of application of force) of the sample.

6. Place a supporting apparatus containing two 1-inch-diameter stainless steel rollers spaced 95 mm apart, center-to-center, on the actuator of an Instron 1331.

7. Place the sample on the apparatus, with its midpoint resting on an extensometer capable of measuring deflections up to 5 mm. Be sure the sample displaces the extensometer when the sample is placed on its rollers. The sample should be oriented such that its label is facing the experimenter.

8. Position the actuator such that the top of the sample is in contact with the Instron's load cell while applying the minimum amount of load possible.

9. Apply a linearly increasing load to the sample by deflecting its midpoint at a constant rate of 0.5 mm per minute via the lowering of a 1-inch-diameter stainless steel roller regulated by an Instron 1331. Acquire data as to the load and deflection applied to the sample via a data acquisition program such as Acqlipse.

10. Record the load experienced by the sample at breakage. Breakage shall be defined to have occurred when the load applied to the sample decreases by a factor of two or more in a period of less than five seconds.

11. Lower the sample using the actuator and remove it from the supporting apparatus. Photograph the fracture of the labeled surface.

12. Hand separate the broken pieces of the sample by approximately 5 mm and photograph the labeled surface again.

13. Photograph the fracture in plan view.

14. Rotate the pieces of the sample 45 degrees about the axes orthogonal to the sanded faces, such that the fracture surfaces are visible to the lens of the camera. Photograph the fracture faces.

15. Label the fractured pieces with a permanent marker and retain them until data analysis is complete.

16. Compute and record the moment at failure according to the equation:

$$M = \frac{PL}{4},$$

Equation 4-1

where

P = Load at failure

L = Distance between midpoints of roller supports

17. Compute and record the modulus of rupture of the sample according to the equation:

$R = \frac{3PL}{2bd^2}$, where

R = Modulus of rupture

b = Width of sample

d = Thickness of sample

Equation 4-2

Figure 4-9 provides photographs of important steps in the process.

Obtain Sample

Soak

Dry

Sand

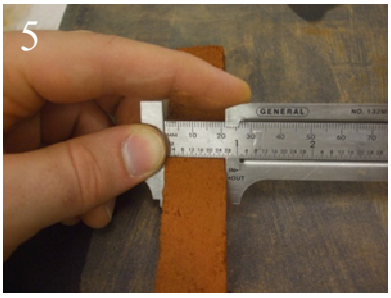

Measure

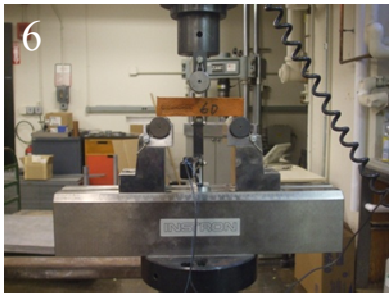

Position 3-Point Apparatus

Load

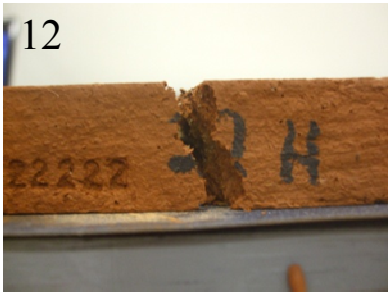

Photo in Elevation

Photo in Plan

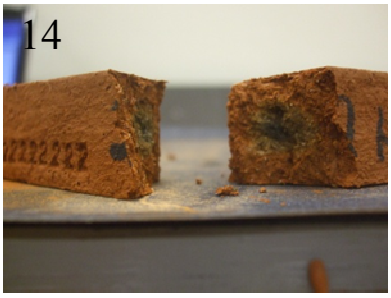

Photo in Isometric

Figure 4-9: Key Steps in the Method of Breaking Samples

4.5.3 A Note on The Precision of The Test Method

Significant figures were carefully considered in the performance of calculations using data from this test.

The load cell has a maximum capacity of ±10 kN, and a signal range of ±10 V. The bit density used in measuring the signal from the load cell was 24, i.e., a 24-digit binary number was used to represent the voltage signal. A 24-digit binary number can represent $2^{24} - 1$ values. Spread over the entire voltage range, this results in a precision of:

$$\text{Precision} = \left(\frac{20V}{2^{24}-1}\right)\left(\frac{1kN}{1V}\right)\left(\frac{1000N}{1kN}\right) = .0012N$$

Equation 4-3

That is to say, the machine is capable of detecting changes in load of magnitude .0012 *N*.

The dimensions of the test specimen were measured using calipers or other instruments capable of measuring to the millimeter. This became the limiting factor in the number of significant digits represented in the results; given that all dimensional measurements were two-digit numbers, two significant digits have been used in the calculation of moment, rupture modulus, and subsequent data manipulations.

5 Results

The fully tabulated results, including dimensions, load at rupture, moment at rupture, and modulus of rupture for all tested samples, appears as APPENDIX D. It will be more instructive, however, to consider the results piecemeal, so as to obtain meaningful comparisons between parameters.

The goal of the bending strength tests is to make statements about the bending strengths of the samples resulting from each compositional or geometrical variation. For such statements to be robust, statistical tests will be employed. An understanding of these tests is key to the interpretation of the results, and a brief description of the relevant tests is therefore presented in APPENDIX E.

5.1 Comparison of Recipes with Compositional Variation

5.1.1 Comparison of Recipes with Incrementally Increasing Combustible Mass

Figure 5-1 presents the moduli of rupture for recipes #1-12[7] as a function of the mass of combustible included in each recipe. Also included are trend lines along with their equations and R^2 values for the four categories of:

1. Rice Husk, No Grog
2. Rice Husk, Grog
3. Sawdust, No Grog
4. Sawdust, Grog

[7] Because recipes 13 and 14 differed in their manufacturing process, their results are handled separately.

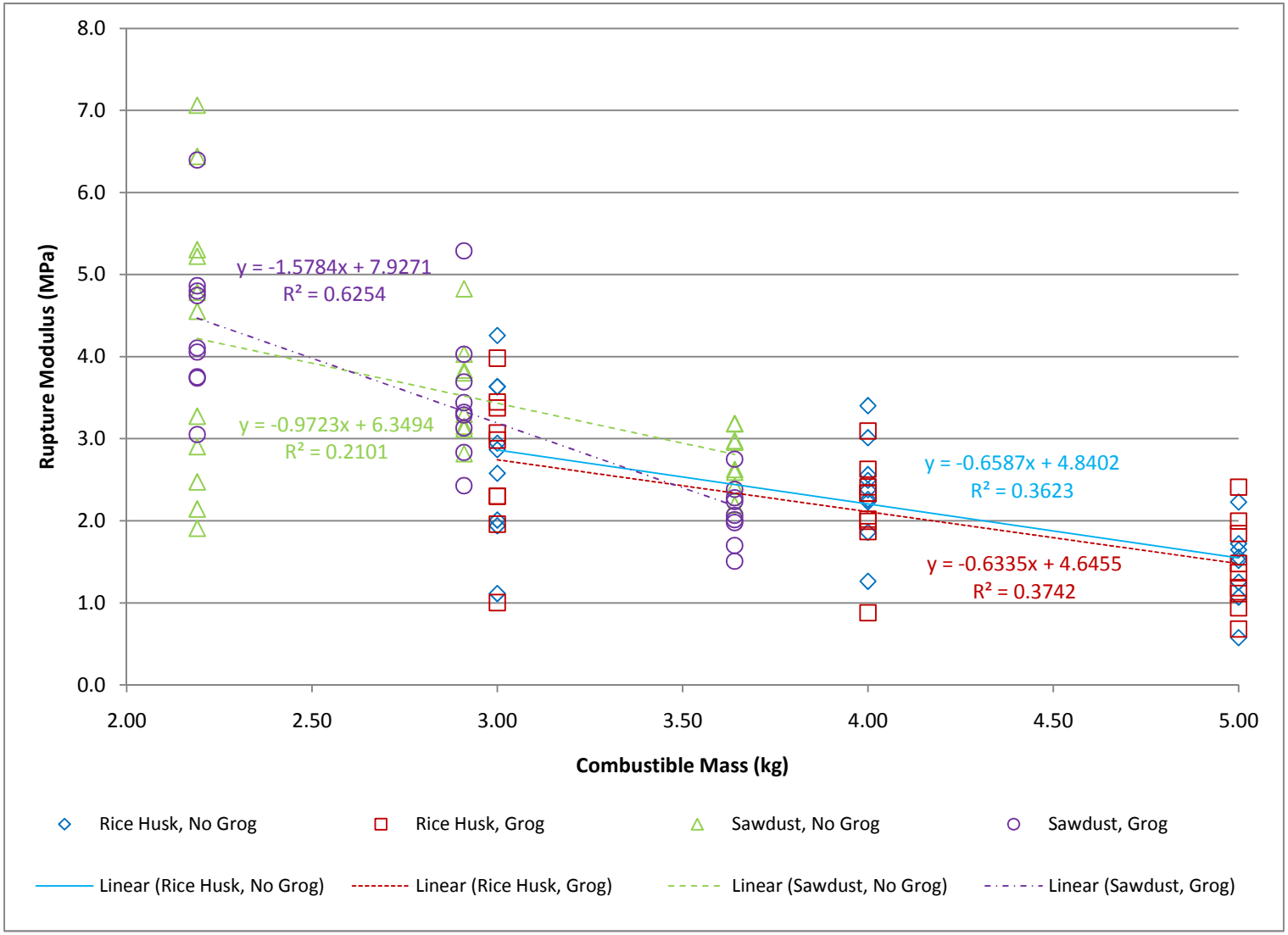

Figure 5-1: Modulus of Rupture vs. Combustible Mass

A number of interesting results may be inferred from this graph. Consider first the change in modulus of rupture with increasing combustible mass. Though linear correlations are poor due to the spread of the data, all four categories display a decreasing relationship between amount of combustible and bending strength. The relationship is more pronounced when viewing all four data sets separately, as in Figure 5-2, or when viewing the means of the data sets, as in Figure 5-3 (note that in this figure, standard error bars representing a 95% confidence interval for the mean are included: convergent solid arrows represent ends of the intervals for rice husk, no grog; flat bars represent ends of the intervals for rice husk, grog; convergent hollow arrows represent ends of the intervals for sawdust, no grog; solid ovals represent ends of the intervals for sawdust, grog).

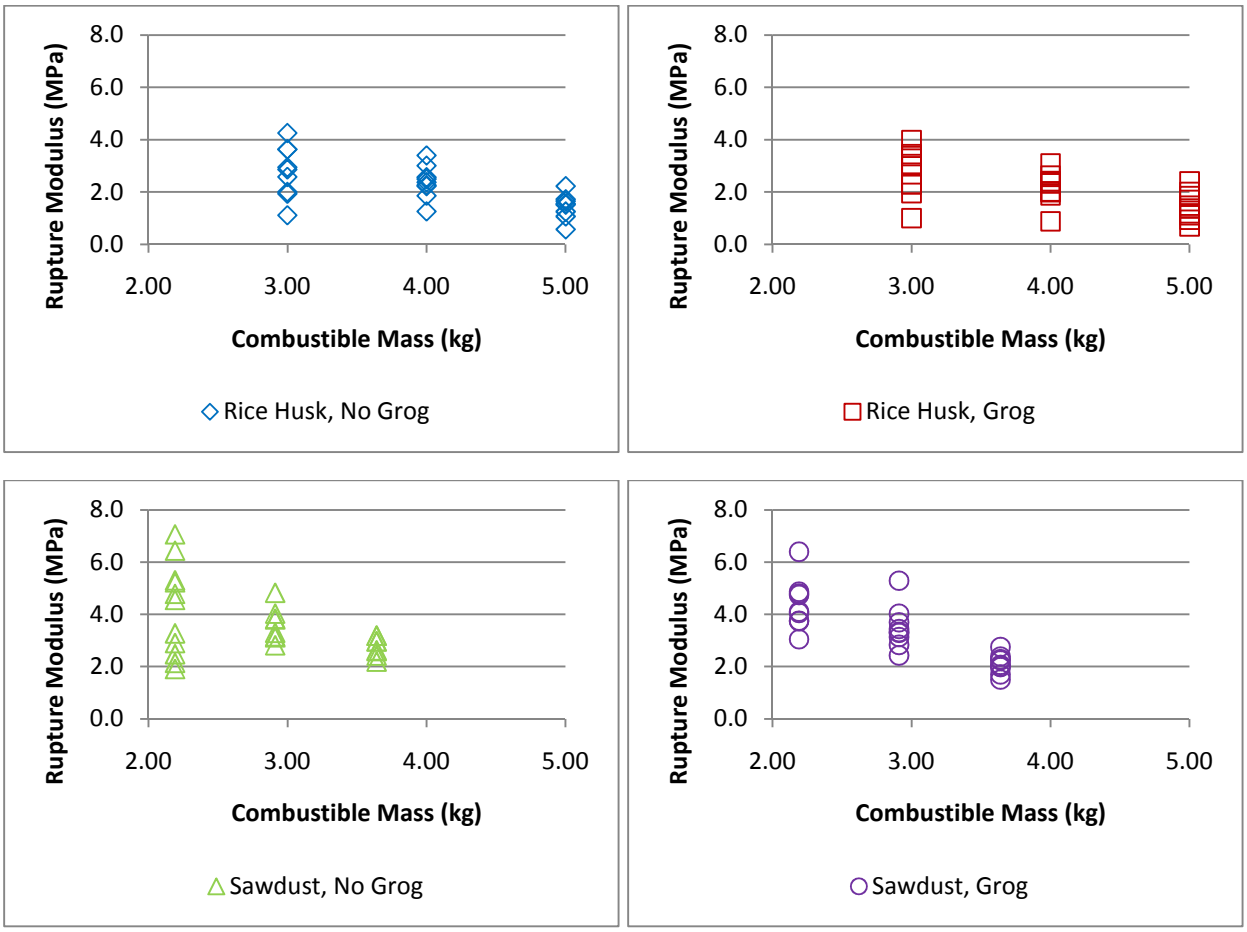

Figure 5-2: Modulus of Rupture vs. Combustible Mass, Separated Categories

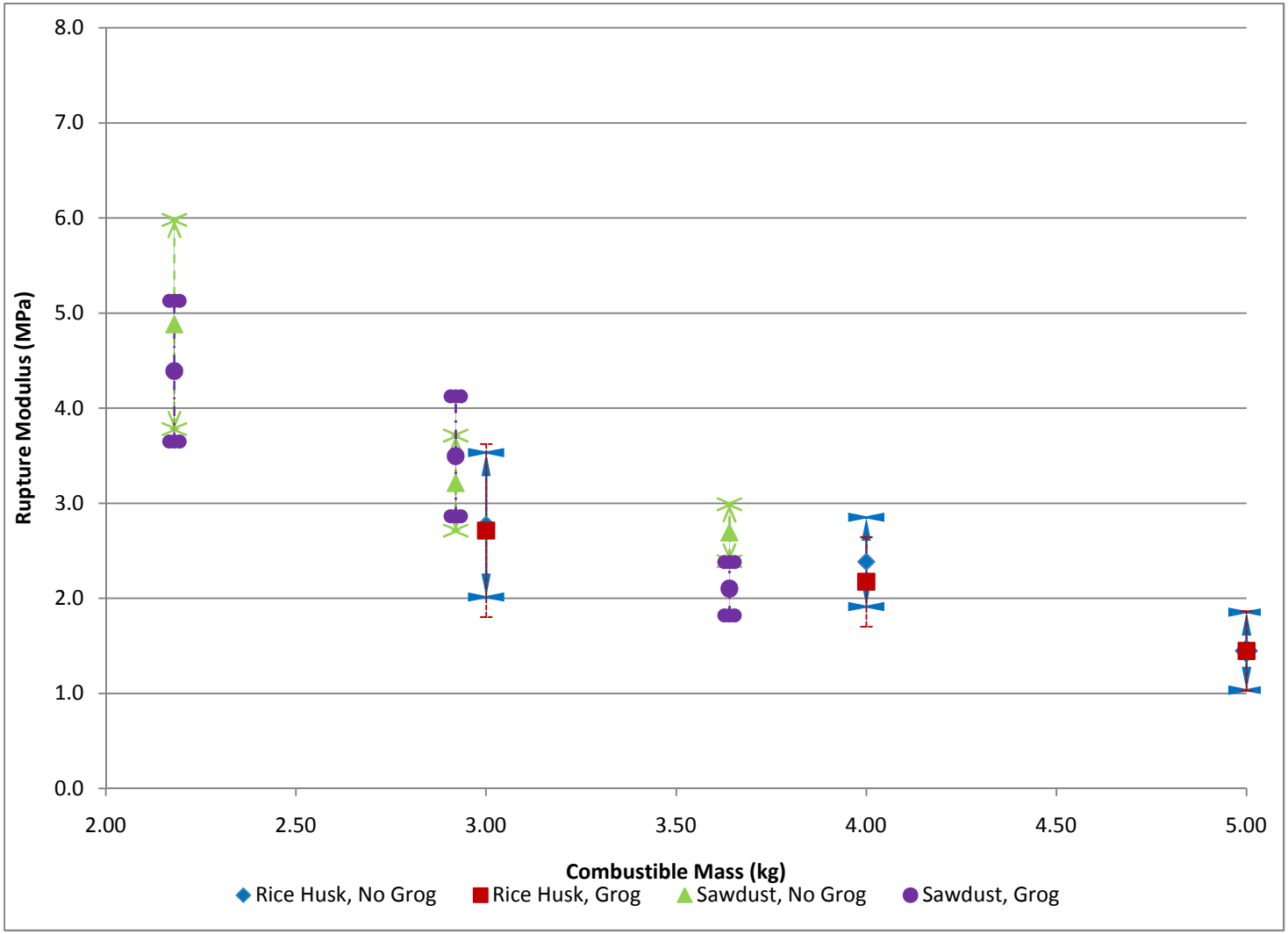

Figure 5-3: Mean Moduli of Rupture vs. Combustible Mass

All four categories display a decreasing relationship between amount of combustible and bending strength. That is, as the combustible mass increases, the bending strength decreases.

The decreasing relationship is well-supported by statistical analysis. One sees from Table 4-1 that recipes #1 and #3 are identical except for the incremental increase in the amount of combustible. Similar statements can be made for the pairs of recipes inTable 5-1, which compares mean moduli of rupture for the pairs of interest.

Table 5-1: Comparison of Mean Modulus of Rupture Between Recipes with Incrementally Differing Combustible Mass, 95% Confidence

Test	T	$T_{.05}$	$t>T_{.05}$?
1>3	1.0	1.746	FALSE
2>4	1.5	1.746	FALSE
3>5	3.4	1.761	TRUE
4>6	2.7	1.746	TRUE
7>9	3.2	1.746	TRUE
8>10	2.1	1.746	TRUE
9>11	2.1	1.746	TRUE
10>12	4.7	1.746	TRUE

For all but the first two tests, one may state with 95% confidence that the incremental increase in combustible mass yields on average a weaker modulus of rupture.

5.1.2 Comparison of Recipes With and Without Grog

Consider Figure 5-4 and Figure 5-5. In each figure, the recipes with and without grog are presented for one combustible type.

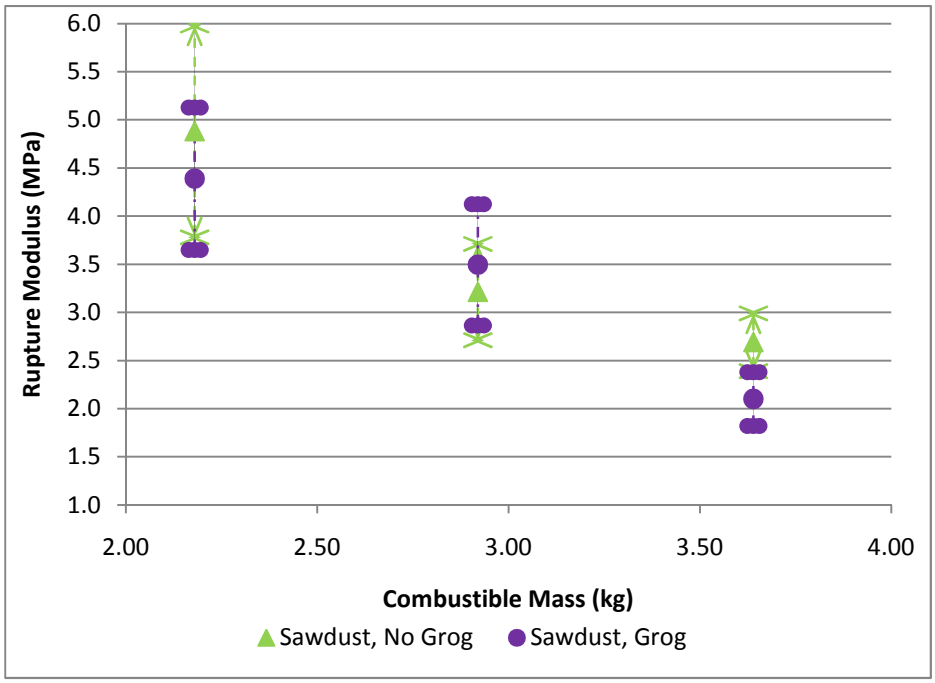

Figure 5-4: Mean Modulus of Rupture vs. Combustible Mass for Sawdust With and Without Grog

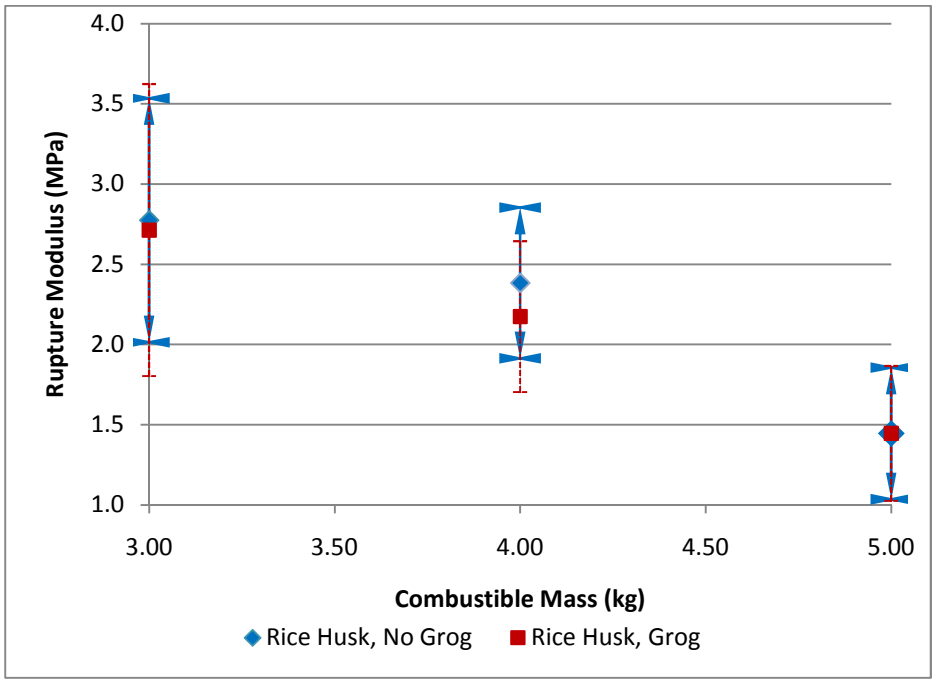

Figure 5-5: Mean Modulus of Rupture vs. Combustible Mass for Rice Husk With and Without Grog

One sees that recipes with grog tend to plot slightly below the recipes without grog. This may imply that the inclusion of grog results in a weaker modulus of rupture. However, a statistical test yields the results presented in Table 5-2.

Table 5-2: Comparison of Mean Modulus of Rupture Between Recipes With and Without Grog, 95% Confidence

Test	t	$T_{.05}$	$t>T_{.05}$?
1>2	0.14	1.746	FALSE
3>4	0.72	1.746	FALSE
6>5	.0011	1.761	FALSE
7>8	0.86	1.746	FALSE
10>9	0.81	1.746	FALSE
11>12	3.3	1.746	TRUE

In only one case does the inclusion of grog create a statistically significant result. In that case (11>12), the inclusion of grog yields a lesser modulus of rupture.

5.1.3 Rank Ordering of Mean Modulus of Rupture

A simple rank ordering of the means of the moduli of rupture is presented in Table 5-3.

Table 5-3: Rank Ordering of Mean Modulus of Rupture

Recipe #	Rank	R_{mean} (MPa)
13	1	6.7
14	2	5.2
7	3	4.9
8	4	4.4
10	5	3.5
9	6	3.2
1	7	2.8
2	8	2.7
11	9	2.7
3	10	2.4
4	11	2.2
12	12	2.1
6	13	1.4
5	14	1.4

However, a recipe of rank n is not necessarily statistically significantly stronger than a recipe of rank $n+1$. To present the results with respect to statistical significance, one may compare a recipe of rank n to each of the recipes of rank $m_i>n$ to determine the recipe of highest mean strength which is still statistically significantly weaker than the recipe of rank n. This creates a tiered ranking structure, in which several recipes may belong to the same tier, wherein they share a recipe of maximum mean strength which is still statistically significantly weaker than the recipes in that tier. Such a tiered ranking is presented in Table 5-4, with Table Table 5-3 reproduced at left for purposes of comparison. The ranks in Table 5-4 are denoted with primes so as to distinguish them from the ranks of Table 5-3.

Table 5-4: Rank Ordering of Mean Modulus of Rupture (at Left); 95% Confidence Tiered Rank Ordering of Mean Modulus of Rupture (at Right);

Recipe #	Rank	R_{mean} (MPa)
13	1	6.7
14	2	5.2
7	3	4.9
8	4	4.4
10	5	3.5
9	6	3.2
1	7	2.8
2	8	2.7
11	9	2.7
3	10	2.4
4	11	2.2
12	12	2.1
6	13	1.4
5	14	1.4

Recipe #s	Rank	Stronger Than:
13	1′	14
14,7,8	2′	10
10	3′	2
9	4′	11
11	5′	4
1,2	6′	12
3,4,12	7′	6
6,5	8′	None

5.1.4 Comparison of Mean Modulus of Rupture to Maximum Expected Stress

For a given recipe, one may ask whether the mean modulus of rupture is likely to be great enough to withstand the expected bending stresses. Recall from Equation 3-14 and Equation 3-15 that the expected bending stress in a pot carrying a full water load is 0.45 MPa, and the expected bending stress in a pot bearing only its wet self-weight is 0.20 MPa. Table 5-5 is a comparison of the lower bound of the 95% confidence interval between the mean modulus of rupture of each recipe and the expected stresses.

Table 5-5: Comparison of Lower Bound of 95% Confidence Interval for Mean Modulus of Rupture to Expected Stresses

Recipe #	Lower Bound (MPa)	Greater than Bending Stress Due to Empty Wet Weight (0.20 MPa)?	Greater Than Bending Stress due to Full Wet Weight (0.45 MPa)?
13	5.8	YES	YES
14	3.9	YES	YES
7	3.8	YES	YES
8	3.7	YES	YES
10	2.9	YES	YES
9	2.7	YES	YES
1	2.0	YES	YES
2	2.0	YES	YES
11	2.4	YES	YES
3	1.9	YES	YES
4	1.7	YES	YES
12	1.8	YES	YES
6	1.0	YES	YES
5	1.0	YES	YES

With 95% confidence, one can say that each recipe will be strong enough, on average, to bear the bending stress induced by its wet self-weight. With 95% confidence, one can say that each recipe will be strong enough, on average, to bear the bending stress induced by its wet self-weight and a full load of water.

One may also ask: what is the probability that a given sample from a particular recipe will yield a modulus of rupture insufficient to bear the expected bending stress? For all recipes, the probability that a sample will be unable to bear its wet self-weight is negligible. The probability that a sample of a particular recipe will be too weak to bear the bending stress induced by its wet self-weight and a full load of water is presented in Table 5-6.

Table 5-6: Probability that the Modulus of Rupture of a Particular Sample from a Given Recipe will be Less than the Expected Bending Stress Arising from A Full Water Load

Recipe #	Probability that R < .45 MPa
13	0.000000
14	0.0026
7	0.0074
8	0.000019
10	0.00010
9	0.000012
1	0.0088
2	0.0067
11	0.000000
3	0.00083
4	0.0021
12	0.000004
6	0.042
5	0.026

5.2 Comparison of Samples with Geometrical Variations

Recall Equation 3-12, which demonstrates the dependency of the maximum stress experienced by a rectangular cross-section of width w and thickness t:

$$\sigma_{max} = \frac{M\frac{t}{2}}{\frac{1}{12}wt^3} = \frac{6M}{wt^2}$$

Recall also that the rupture modulus, R, is the maximum stress that can be withstood by a cross-section of a given material. Replacing σ_{max} with R in Equation 3-12, one may rearrange to demonstrate the dependency of the critical moment (i.e., the moment at which rupture is expected to occur) on the thickness of the cross-section:

$$M_{critical} = \frac{Rwt^2}{6}$$

Equation 5-1

Theoretically, then, for samples of identical width and modulus of rupture, one would expect a graph of the critical moment to increase with the square of the thickness. Figure 5-6 presents the theoretical curve for the samples manufactured from recipe #4; the average sample width and average modulus of rupture were used as coefficients. The experimental data are also plotted, with a corresponding power curve graphed for comparison.

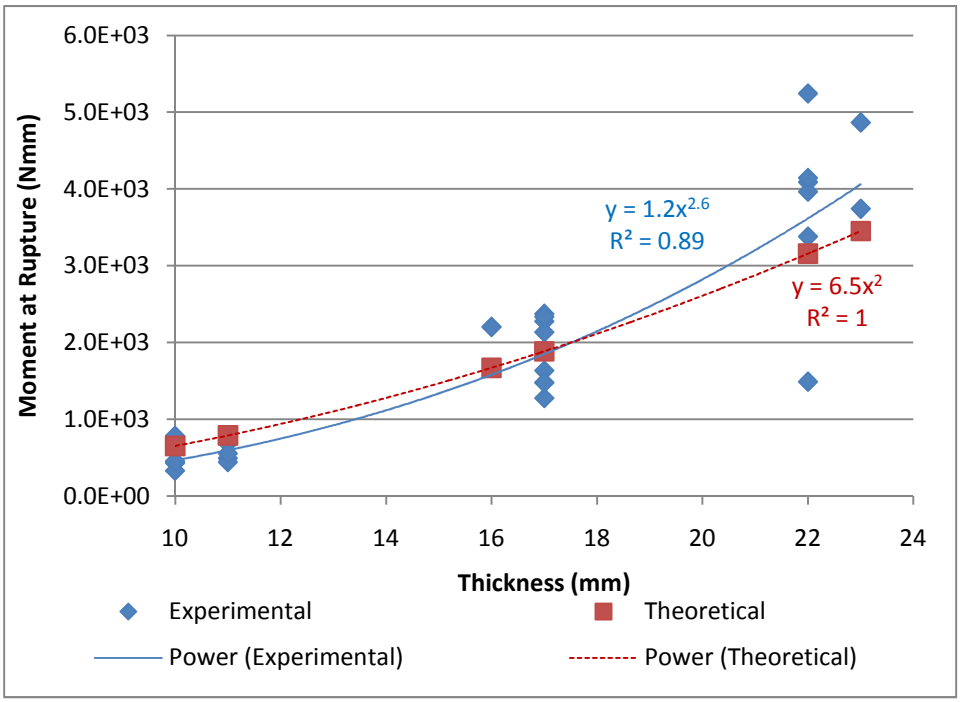

Figure 5-6: Moment at Rupture vs. Thickness for Samples Manufactured from Recipe #4

Though the curve deviates from the theoretical, the R^2 value for the given power relationship exceeds R^2 values obtained by assuming a linear, exponential, or order-2 polynomial relationship, suggesting that the power relationship is the best fit for the data.

Given that the known theoretical relationship predicts a dependency on the square of the thickness, rather than the thickness to some fractional power, one is loath to use the equation of the trend line arising from the experimental data in predicting strength changes based on thickness. However, the relationship does suggest that the data obeys the theoretical prediction, and at least quadratic gains in allowable moment will be realized when thickening the lip of the filter.

Table 5-7 is presented in statistical support of the gain in allowable moment realized when thickening the samples.

Table 5-7: Comparison of Allowable Moment for Samples of Varying Thickness, 95% Confidence

Test	t	$T_{.05}$	$t>T_{.05}$?
$M_{max,medium}>M_{max,thin}$	9.8	1.746	TRUE
$M_{max,thick}>M_{max,medium}$	4.7	1.746	TRUE

5.3 Caveats in the Interpretation of Results

5.3.1 Physical Caveats

5.3.1.1 The Effect of Kiln Position on Modulus of Rupture

All samples were fired in the same firing in hopes of minimizing any variations due to differential heating. Unfortunately, even within the same kiln, one finds that some areas experience different heating properties than others. This differential heating is evidenced by the behavior of pyrometric cones included in the kiln during the firing.

Pyrometric cones provide a method for the measurement of heat absorption (Nidec-Shimpo America, 2009, p. 9). The cones are manufactured in such a way that they bend to a known angle after a known amount of heat absorption. Though a temperature measurement cannot properly be applied to the cones, given that they measure heat absorption and not temperature, most manufacturers provide an approximate temperature correlation for each cone. Thus, one may speak of cones being "hotter" or "cooler" than one another.

Pyrometric cones are often employed in groups of three – the guide cone, the firing cone, and the guard cone. The guide cone is one cone cooler than the firing cone; its bending indicates that the samples inside the kiln are nearing maturity. The bending of the firing cone indicates a completed firing. The guard cone is one cone hotter than the firing cone. One usually does not intend for the guide cone to bend, but should this occur, the angle of bending will provide a measure of the degree to which maturity has been exceeded (Nidec-Shimpo America, 2009, p. 9).

Table 5-8 gives the cone number and associated temperature value for the Nidec-Shimpo America Corporation cones used in the firing of the ceramic samples.

Table 5-8: Cone Numbers and Corresponding Temperatures Used in the Firing of the Ceramic Samples

Cone Number	Corresponding Temperature (°C)
012	901
011	883
010	871

Figure 5-7 is a photograph of the pyrometric cones after the firing, with their relative positions maintained, along with a reproduction of Figure 4-7.

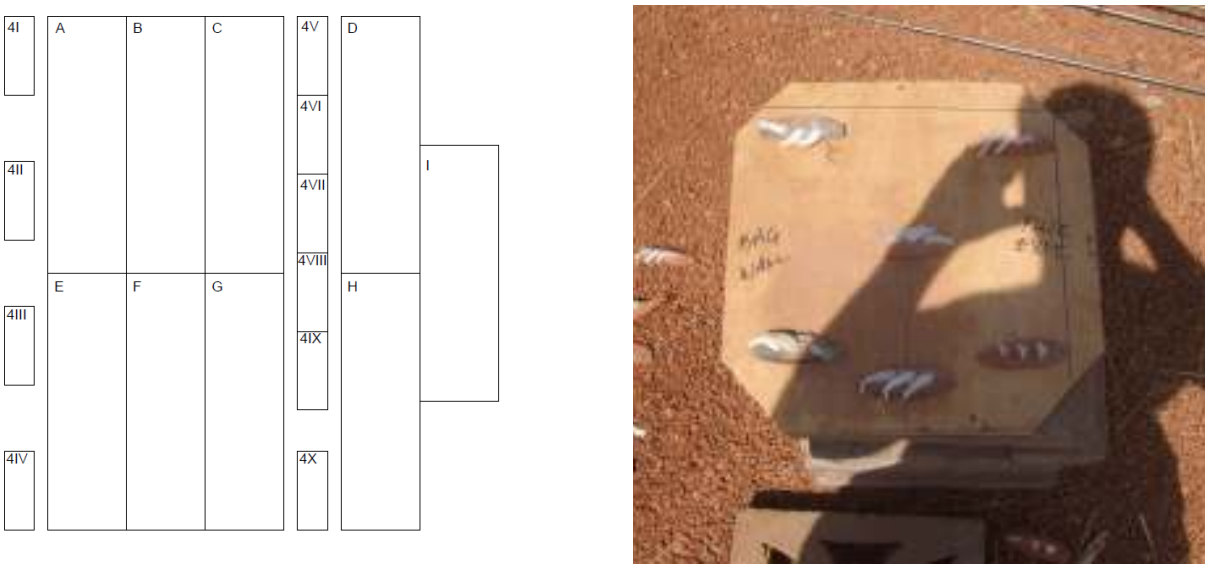

Figure 5-7: Schematic of Kiln Loading (Left) and Photograph of Pyrometric Cones Taken After Firing with Relative Positions Preserved (Right) (Watters 2010)

The cones in the upper left-hand corner of the photograph were positioned at the upper left-hand corner of the kiln floor, in position A. The cones in the upper right-hand corner were positioned at the upper right-hand corner of the kiln floor, in position D. The cones in the lower right-hand corner were placed in the lower right-hand corner of the kiln floor, in position H. The cones in the lower left-hand corner were placed in the lower left-hand corner of the kiln floor, in position E. The cones in the center were placed in the center of the kiln floor, between positions B and F. The remaining set of cones was elevated in the kiln door.

One sees that in all positions except for *H*, the cones have melted and bent. In position *H*, not even the guide cone has bent. This implies that in all positions except for *H*, the samples exceeded maturity. The greatest degree of maturity is witnessed in position *E*, where the cones are not only bent, but completely melted.

Figure 5-8 is a graph of modulus of rupture vs. combustible amount for the entire data set of ≈22mm thick samples, organized by kiln position.

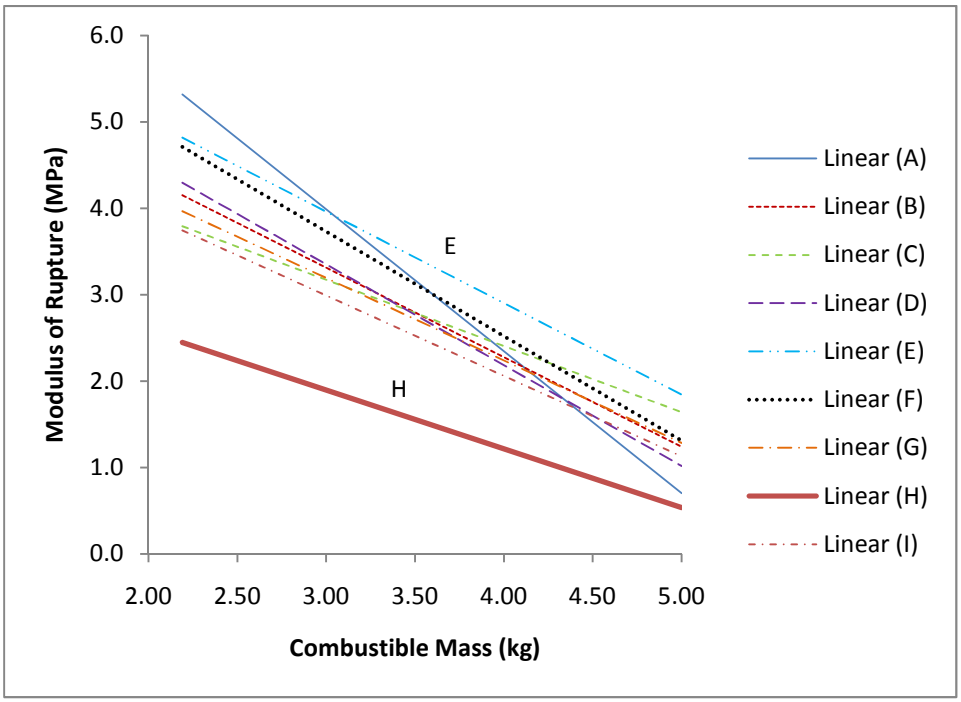

Figure 5-8: Modulus of Rupture vs. Combustible Mass Trend Lines for Each Kiln Position

One notices that, while many of the lines are clustered toward the center of the graph, indicating only a small variation in strength with temperature, the trend line for the samples in position *H* graphs well below the trend line for position *E*. In fact, comparing their mean values, one finds that the mean strength of the samples from position *E* exceeds the mean strength of samples from position *H* with at least 95% confidence. Recipe #1 provides a particularly dramatic case, in which the sample at *E* exhibited a 3.6-fold strength increase compared to the sample at *H*.

A relationship between firing maturity and strength cannot be derived from the available data. It is clear, however, that samples of a lesser maturity tend to exhibit lesser rupture moduli.

5.3.1.2 Uncertainty of the Failure Mechanism

In a three-point bending test, the load, shear, and moment diagrams may be represented as follows:

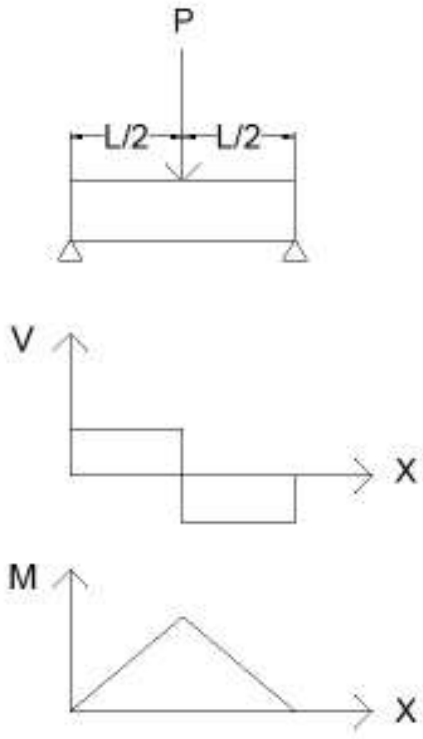

Figure 5-9: Load (Top), Shear Force (Middle), and Moment (Bottom) in a Three-Point Bending Test

The tested specimens failed at or near the midspan of the beam, where moment is at a maximum and the shear force is changing direction. This implies that bending is the primary mechanism causing failure of the tested specimens. Most of the fracture surfaces exhibited vertical or nearly vertical failure planes, which supports the assumption that bending stress is responsible for the failure. Sample 13G is presented as an example of a vertical failure plane in Figure 5-10.

Figure 5-10: Vertical Failure Plane Exhibited by Sample 13G

Some samples, however, failed at an angle, implying either preferential crack propagation along planes of imperfection or the influence of shear stress. Sample 13H is presented in Figure 5-11 as an example of an angled failure plane..

Figure 5-11: Angled Failure Plane Exhibited by Sample 13H

Let us assume that the beam is bearing its maximum shear force at the same time and location as the moment force it experiences during rupture. If shear is indeed influencing the failure, then a beam subjected to pure bending would fail at a moment greater than the recorded moment. Assuming that the observed modulus of rupture is the true modulus of rupture is therefore conservative but inaccurate.

Furthermore, one may compare this shear force to the maximum shear force expected from the full-pot loading condition. One finds that, for all samples cast with the 25 mm-thick mold, the shear experienced at failure exceeded the shear predicted from the full-pot loading condition, with one exception: recipe #6H sustained a shear stress of 0.052 MPa at failure. All other 25 mm-thick samples exceeded the shear stress from the full-pot loading condition by a factor of 3.6 on average. Even while bearing a moment load far greater than the expected moment from the full-pot loading condition, the recipes were able to bear a shear far greater than the expected shear from the full-pot loading condition.

This is not the case for the thin (13 mm) samples. The average shear stress at failure for the thin samples, which were created using recipe #4, is 0.049 MPa. The bending stress at failure for the thin samples still exceeds the expected bending stress by a factor of at least 2 for all tested samples. The test is designed to place the sample in bending, not shear, so the fact that the shear at failure in the tested sample is less than the shear expected from the common loading condition does not imply that the lip will fail due to shear under the common loading condition. However, it does forbid us from eliminating shear as the failure mechanism observed in the field.

5.3.2 Statistical Caveats

In the performance of the T-tests comparing the means of two populations, three assumptions are made:

1. The samples are selected from the populations in a random manner.
2. The samples are selected in an independent manner from the two populations.
3. Both of the populations from which the samples have been selected have relative frequency distributions that are approximately normal

One wishes to apply the conclusions drawn from the sample sets obtained at the PHW factory to the population of any future fired samples. However, the only samples for which data have been obtained are samples from a single firing. Indeed, this was done intentionally in order to try to isolate the variables regarding recipe and thickness from those regarding firing conditions. Since variations in bending strength due to firing conditions have been demonstrated even within the same firing, variations in bending strength due to firing conditions is expected across different firings. Thus, the samples selected are not representative of all samples that may be produced at the PHW factory, and the first assumption has been violated. Therefore statements regarding the absolute modulus of rupture for samples of a given thickness and recipe are not justified across a population spanning multiple firings, though the relative strength correlations are justified across the single firing. In order to make statements about relative strength regarding all firings, one must assumed that the relative strength correlations will be unaffected by differing firing conditions, i.e., variations in firing conditions will affect the strength of all samples identically.

The selection of one sample in no way affected the selection of a second sample; therefore the samples were selected in an independent manner and assumption 2 was upheld.

Mendenhall and Sincich suggests several methods for determining whether selected data are from an approximately normal distribution (2007, p. 185). One such test involves the fraction *IQR/s*, where *IQR* is the interquartile range and *s* is the standard deviation. If the data are approximately normal, this value is approximately equal to 1.3. Table 5-9 lists this quotient for the several data sets considered in this thesis.

Table 5-9: IQR/s Values for Data Sets Used in Statistical Comparisons

Data Set	IQR/s
Recipe #1	1.6
Recipe #2	1.2
Recipe #3	0.54
Recipe #4	0.68
Recipe #5	0.94
Recipe #6	1.3
Recipe #7	0.53
Recipe #8	1.1
Recipe #9	1.3
Recipe #10	.69
Recipe #11	1.4
Recipe #12	0.82
Recipe #13	0.80
Recipe #14	1.1
Recipe #4 Thin	1.6
Recipe #4 Medium	1.6
Kiln Position E	1.3
Kiln Position H	1.5

In some cases, the value *IQR/s* is approximately equal to 1.3, and in others it is not. This is not entirely unexpected, given that, even if the data were normally distributed, a sample size of 9 (in the case of recipes #1-4, #6-13, #4 Thin and #4 Medium), 8 (in the case of recipe #5), or 14 (in the case of kiln positions E and H) is small. If the sample size were increased, the data sets may approach a more normal distribution; still, the possible deviation from normality should be noted when considering the stated results.

6 Recommendations and Conclusion

6.1 Recommendations for Pure Home Water

6.1.1 Compositional Recommendation

The strength of the material compositions has been ranked by simple mean and by statistically significant mean comparisons in Table 5-3 and Table 5-4, respectively. However, the filter recipe must also be evaluated on the criteria of flow rate and removal efficiency. As previously mentioned, Miller (2010) performed a parallel twelve-week study evaluating the flow rate and removal efficiency of the recipes given in Table 4-1. One of the results of his work was a statistically significant ranking comparison for each of the characteristics of flow rate, *E. coli* removal, and Total Coliform removal, performed following the same methods described in Section 5.1.3 for statistically significant ranking of mean strength.

A simple table integrating the author's and Miller's results is presented as Table 6-1. A rank has been assigned to each recipe on the criteria of strength, effluent *E. coli* concentration, flow rate, and total coliform removal. For this analysis, recipe #13 was excluded – although its strength was greatest, it stopped flowing shortly after production, rendering it useless. Summing the ranking for each of the recipes yields a total score. A minimum score implies an optimum recipe.

Table 6-1: Ranking Table Integrating Several Tested Parameters

Recipe #	Strength	Flow Rate Ranking	E. Coli	Total Coliform	Total Score
1	5	4	2	3	14
2	5	5	1	2	13
3	6	3	1	3	13
4	6	3	1	4	14
5	7	2	1	3	13
6	7	1	1	5	14
7	1	7	3	5	16
8	1	7	2	5	15
9	3	7	1	5	16
10	2	7	3	4	16
11	4	5	2	5	16
12	6	4	1	4	15
14	1	5	1	5	12

One sees that recipes # 14 has the lowest ranking. Unfortunately, the manufacturing process involved in recipe #14 is cumbersome – milling *and* sieving is particularly labor-intensive, and the rice husk tends to form a caked mass on the sieve, rather than sieving easily. This leaves recipes #2, #3, and #5, which share the lowest ranking. New criteria must be applied to select between these, effectively suggesting a weighted ranking.

Recipe #2 includes grog, which implies a labor and material cost for which there is, as yet, no observed advantage. Furthermore, its flow rate is significantly worse than recipes #3 or #5. This recipe is therefore dismissed.

Recipe #5 belongs to the weakest tier of tested recipes. All else being equal, one would prefer not to use the weakest of all recipes in filter production. Recipe #5 is therefore dismissed.

Of the recipes tested, the author recommends that recipe #3 is the most appropriate for future production. The reader may revisit Sections 4.1 through 4.4 for information as to the preparation and composition of this recipe.

6.1.2 Geometrical Recommendation

Section 5.2 demonstrated that, at minimum, one should expect lip bending strength to increase as the square of the thickness of the lip. It is therefore recommended that Pure Home Water thicken the lip of the filter. Thickening the lip to 20 mm will result in factors of safety regarding bending strength of, on average, 2.4, while thickening the lip to 25 mm will result in factors of safety regarding bending strength of, on average, 4.5. Such an increase will still allow the top lid to overhang the ring lid, thereby limiting the path of possible contamination to the water in the pot. Furthermore, this thickness is not so great as to create a cumbersome pot. Thickening the lip to 25 mm will result in dramatic increases in both bending strength and shear strength while increasing the material volume by 10%. It is the author's recommendation that the lip be thickened to 25 mm.

If material costs are of concern, the lip may also be designed with a taper, such that it reaches its maximum thickness only at the point of adjoinment with the filter wall. Such a design is presented in Figure 6-1.

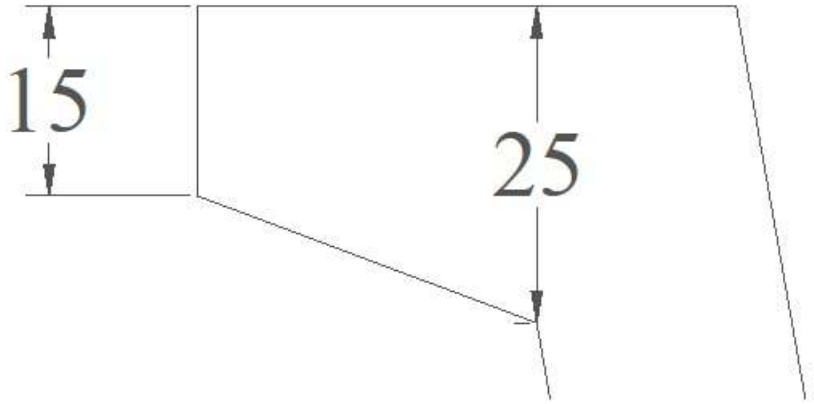

Figure 6-1: Possible Lip Geometry

This geometry would result in identical strength gains in shear and moment at the critical location for a 5% material increase. The resulting filter may, however, be more difficult to handle and will not rest as easily within the plastic ring. It is therefore not recommended that this design be adopted.

6.1.3 Firing Recommendations

As seen in Section 5.3.1, variations in firing can drastically impact the strength properties of the finished product. The qualities of the finished product depend not only on the final temperature of the material, but upon its total heat absorption.

After the first four hours of firing, the witness cones in the spyhole and in the door of the kiln must be checked no less than hourly. Once the guide cone has bent, the witness cones should be checked at least once every 15 minutes. These time increments may be adjusted with experience, as workers begin to develop experience with the behavior of the witness cones. The crucial precept that must be communicated is the dependence of the finished product on heat absorption rather than instantaneous temperature.

Also clearly demonstrated in Section 5.3.1 is the variation in temperature with position in the kiln. The author recommends that Pure Home Water make every effort to monitor and enforce the uniformity of the firing in the kiln. The author recommends that witness cones be used in every firing and that their condition at the end of firing and their position be documented photographically. Communication must be maintained with the kiln designer, Manny Hernandez, to implement changes to the interior configuration of the kiln in order to create a more even heat distribution.

6.2 Recommendations for Further Research

6.2.1 Data Acquisition

In attempting to improve the durability of the CPF, difficulties arose due to the lack of information as to the failure modes causing breakage of the pot. During subsequent follow-up monitoring investigations, it is recommended that:

1. A photo log of broken pots be maintained, including plan and isometric views of the fracture surface(s).

2. User testimony as to the conditions of failure should be recorded.

3. All pieces of fractured pot should be recovered, and pieces from the same pot be maintained together, distinctly from pieces from other pots.

Collection of such information will facilitate determination of primary failure mechanisms and targeted efforts to strengthen future CPFs against said mechanisms.

6.2.2 Compositional Recommendations

Testing of the 14 aforementioned recipes yielded useful information but left many questions unanswered. The experiments performed herein and by Miller (2010) may be repeated with slight variation to address unresolved issues:

1. Compositions with identical masses of rice husk and sawdust should be tested, with finer divisions in the mass of sawdust and rice husk. This will reveal whether statistically significant strength gains may be realized by preferentially using one combustible type, and will provide more information as to the nature of the relationship between strength and combustible mass (linear, quadratic, etc.)

2. Recipes #13 and #14, with the unique manufacturing process of milled, sieved combustible, yielded the strongest mixes. Their filtering rates, however, were unacceptable. Being that there is a demonstrated relationship between flow rate and combustible mass, the manufacturing process used in recipes #13 and #14 should be applied to various other recipes with higher proportions of combustible. This will reveal whether the strength gains realized in the manufacturing process can be coupled with an acceptable flow rate.

3. After the filters were fired and cooled, they were dipped in a solution of colloidal silver. This treatment was not applied to the tested beams. It is not expected that the colloidal silver decreases the strength properties of the filter. However, if PHW continues to observe lip failures after the implementation of the author's recommendations, retesting with silver-impregnated beams may be of interest.

6.2.3 Impact Strength Testing

It would of course be fortunate if the increases in bending strength due to compositional variation were accompanied by increases in impact resistance. One may confirm or deny this phenomenon by employing the ASTM C368-88, Standard Test Method for Impact Resistance of Ceramic Tableware, as mentioned in Section 3.1.5.1. However, until impact failures from pots made with the recommended compositional and geometrical alterations are observed, it is not recommended that this test be performed.

6.2.4 Development of Shear-Moment Failure Envelope.

Shear stress and bending stress often act in tandem to fail a material. For this reason, it is often of interest to develop a shear-moment failure envelope of the kind shown in Figure 3-9. Unfortunately, full development of this curve is difficult, as it requires an experimenter to either fix the shear stress and alter the bending stress or fix the bending stress and alter the shear stress.

The three-point bending test employed in this thesis does not place the material in pure bending, i.e., bending in which the shear stress is zero. Furthermore, the angular failure planes on the tested samples suggest that, while bending stress is the primary failure mode, shear stress also plays a role in the material's failure. A four-point bending test, whose configuration is shown in Figure 6-2, places the material in pure bending between the two load applicators.

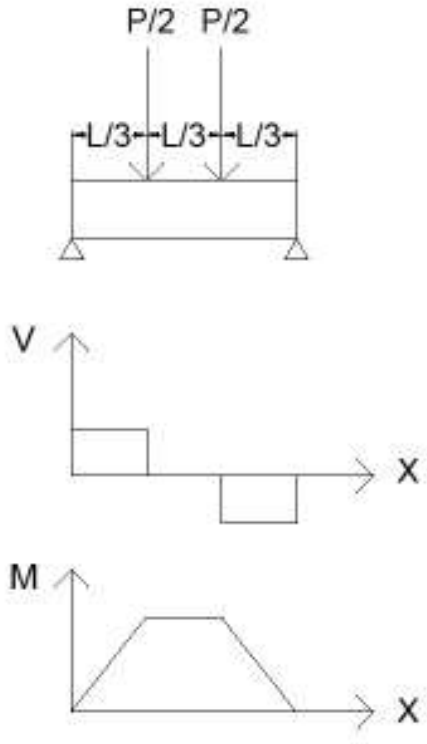

Figure 6-2: Load (Top), Shear Force (Middle), and Moment (Bottom) in a Four-Point Bending Test

Through this test, a more accurate value of maximum bending stress may be determined.

Tests for shear strength of brittle materials are more difficult to design. Consultation with materials scientist and structural engineers should be undertaken if the design of such a test is pursued. The result of the shear test should be a value for the maximum in-plane shear stress that the material can withstand.

Once these two values have been determined, a conservative failure envelope may be drawn as a straight line between the shear and bending strengths. Such a figure is depicted schematically in Figure 6-3.

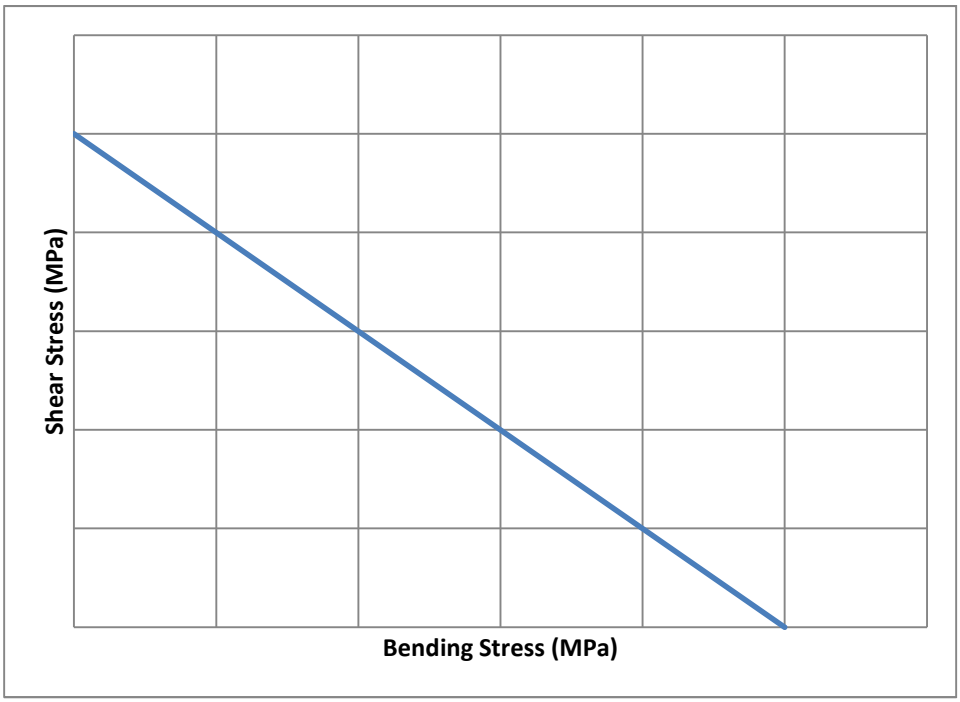

Figure 6-3: Schematic of a Conservative Shear-Bending Interaction Diagram

Though the true failure envelope most likely decreases as a concave-down arc from the maximum shear stress to the maximum bending stress, thereby encompassing more points than the presented envelope, designing within the presented envelope is more likely to prevent shear or moment failures.

In truth, such an analysis is not yet necessary for the improvement of the Pure Home Water filters. If the recommendations suggested thus far do not yield appreciable reductions in lip failures, such a characterization may be of interest.

6.2.5 Development of a Finite Element Model

The experiments suggested in Section 6.2.1 are still limited by:

1. The application of beam theory on a rectangular cross-section as an approximation for the stresses experienced by the lip of the filter.

2. The neglect of shear forces on the faces exposed by removal of the beam from the pot.

For a more accurate characterization of the forces experienced by the pot, and for better predictive capability as to whether or not the lip of the filter will fail under a given loading, the author suggests the application of a numerical analysis method, such as the development of a Finite Element Model.

Development of such a Finite Element Model is not yet in the interest of Pure Home Water and may never be needed. If the recommendations provided thus far do not sufficiently reduce lip failures in the field, development of a Finite Element Model may be of interest.

6.3 Conclusion

A summary of the conclusions drawn from the preceding research is as follows:

1. In six out of eight pairwise comparisons, one may state with 95% confidence that increasing the mass of combustible decreases the mean bending strength of the resulting material.

2. In five out of six pairwise comparisons, there is insufficient evidence to state with 95% confidence that the inclusion of grog results in different mean moduli of rupture. In one out of six pairwise comparisons, one may state that the inclusion of grog results in a weaker mean modulus of rupture with 95% confidence.

3. The recipe whose mean modulus of rupture is, with at least 95% confidence, greater than the mean modulus of rupture of any other recipe, is recipe #13, containing 1.82 kg of fine, sieved sawdust without grog.

4. With 95% confidence, one may state that the mean modulus of rupture for all tested samples exceeds the requisite modulus of rupture arising from a full water load acting on the lip of the CPF.

5. The maximum probability of a filter of a given recipe yielding a modulus of rupture less than the requisite modulus of rupture arising from a full water load acting on the lip of the CPF is 0.042.

6. Experimental evidence supports the theoretical dependence of maximum allowable moment on the thickness of the material raised to at least the second power.

7. Even within the same firing, variation in firing conditions may produce a 3.6-fold difference between identical recipes in different kiln positions.

In light of these conclusions, it is recommended that:

1. The lip of the filter be thickened to 25 mm.

2. Firing be monitored with pyrometric cones placed in the kiln door and spyhole at intervals of one hour after the first four hours and at intervals of 15 minutes after the guide cone has bent. These intervals may be adjusted based on field experience.

3. Recipe #3 be utilized for production in the immediate future.

4. The manufacturing processes used for recipes #13 and #14 be employed on samples of increasing combustible amount and tested for bending strength, flow rate, and removal efficiency.

5. Grog be excluded from the filter recipes unless its inclusion should be demonstrated to improve filters in a way not considered by the research of the author or Miller (2010), such as the reduction of cracking during the drying phase of production.

APPENDIX A: Methods of Measurement

Two (approximate) halves of one broken pot were used for the measurements listed in Table 3-1.

Lip Thickness

Vernier calipers were used to take three measurements around the rim of each half-pot; one measurement was taken near each fracture surface and one was taken near the midpoint of the arc. The average of six measurements was taken as the lip thickness.

Base Inner Diameter:

Each half-pot was measured across its inner cross-section, anchoring the metal end of a semi-rigid mylar measuring tape against one inner edge and stretching the other end, approximately flat across the bottom, until it reached the other inner edge. The midpoint of the tape was taken as the center of the pot.

From this midpoint, the metal hook was placed against the fractured base of the pot, and the tape was stretched along a line perpendicular to the fracture line until it met flush with the inner edge of the pot. The tape was held down with a fingernail, and the last mark to rest flat against the base of the pot was recorded as the length from the center to the outer edge.

This was repeated on the other half-pot, and the sum of the two lengths was recorded as the diameter. The average of three measurements was taken.

Base Outer Diameter

The two halves of the pot were pressed together and placed rim-side-down on a flat surface. The metal end of a semi-rigid tape measure was hooked over one side such that the centerline of the tape approximately coincided with the center point of the pot's base. The tape was rotated along the base of the pot until the distance read on the tape reached a maximum value. The free end of the tape was bent to match the angle of rise of the pot. The point at which the tape's angle matched the angle of rise of the pot was taken as the outer diameter. The average of three measurements was taken.

Base Thickness

Three measurements were taken by Vernier caliper along the line of fracture for both pots. One measurement was taken near one edge, one near the middle, and one near the other edge. The average of six measurements was taken as the base thickness.

Width of Lip

The metal hook of the mylar tape was held flush against the bottom underside of the lip and pressed against the outer surface of the pot. The other end was stretched to the outermost part of the lip, and the measurement was taken as the first visible marking on the tape when sighted from directly above. Three measurements were taken per each half-pot

Slant Height

The fractured surface of the pot was placed against a flat table. The metal hook of the mylar tape was anchored at the bottom of the pot, stretched against the pot's outer surface, and held flush against the underside of the lip. The tape was rotated about the hooked end until a minimum value was read at the underside of the lip. The last marking to be held flat against outer surface was recorded as the slant height. An average of two measurements (one for each half-pot) was taken.

Angle of Rise

The pot was placed on its bottom with the plane of its fractured surface coincident with the edge of a flat table. A protractor was held against the table with its centerline marking the last point at the bottom of the pot's outer edge before the edge began to curve into the fillet at the bottom outer edge of the pot. The outer edge of the pot was sighted and measured as the angle of rise. An average of four measurements – one for each outer edge – was taken.

APPENDIX B: Measurements of CPFs from Several Locations

As mentioned in Section 3.2.1, van Halem has produced a summary of measurements for several types of CPF. Her summary is presented here alongside the author's measurements pertaining to the PHW CPF. Figure 3-1 is reprinted here for purposes of clarity.

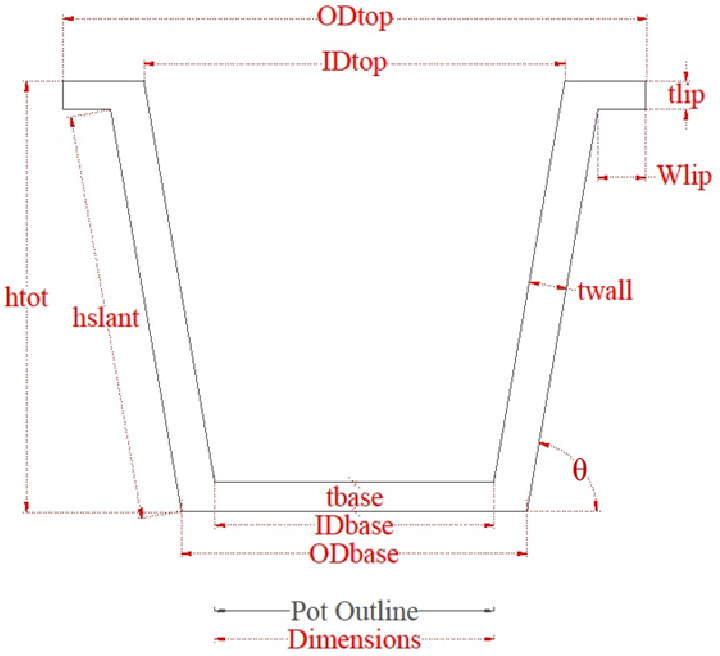

Measurement	CPF Type			
	PHW Ghana	*Ceramica Tamakloe Ghana*	*Cambodia*	*Nicaragua*
OD_{top}	30.7 cm*	---	---	---
ID_{top}	22.2 cm*	---	---	---
OD_{base}	18.2 cm	22.6 cm†	22.7 cm†	24.6 cm†
ID_{base}	14.7 cm	20.0 cm	19.5 cm	22.0 cm
t_{lip}	1.5 cm	---	---	---
t_{wall}	2.0 cm*	1.3 cm	1.6 cm	1.3 cm
t_{base}	1.5 cm	1.5 cm	1.4 cm	1.7 cm
h_{tot}	22.7 cm*	---	---	---
h_{slant}	21.5 cm	25.3 cm†	25.2 cm†	23.8 cm†
W_{lip}	2.5 cm	---	---	---
Θ	80°	81.5°†	81.5°†	84.2°†

**Value obtained from AutoCAD© 2010*
---Value not provided by van Halem and not calculable from van Halem's provided values
†Value not provided by van Halem but calculated from van Halem's provided values

APPENDIX C: Derivation of the Location and Magnitude of the Maximum Moment Experienced by the Lip of the Ceramic Pot Filter

Recall the loading condition described in Section 3.2.2

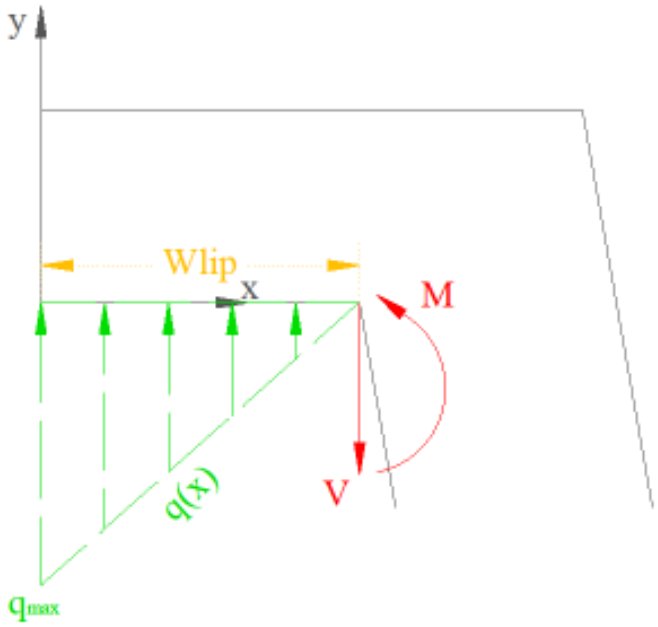

One treats the intersection of the lip with the filter wall as a cantilevered support, incapable of displacement or rotation and thus exerting a shear and moment reaction. Note the new coordinate system, with the *x*-axis oriented along the dimension of the lip's width, and the *y*-axis perpendicular to the *x*-axis. Furthermore note that q_{max} is the maximum value of the linearly decreasing distributed load *q(x)*, which decreases to zero over the distance W_{lip}. That is, the load function has slope $m = q_{max} / W_{lip}$.

The quantities of interest are the magnitude and location of maximum moment on the lip of the filter. It is well-known that the moment function is equal to the integral of the shear function, and that the integral of the load function is the shear function (Beer, Johnston Jr., & Eisenberg, 2004, pp. 372-373). One may first describe the load distribution function, then integrate twice and apply boundary conditions to solve for the moment function. We may use this information to determine the location and magnitude of the maximum moment.

Determination of the Load Function

R is the force whose magnitude is equal to the sum of all forces represented by the distributed load. Therefore, *R* is the area under the curve of the distributed load. Since the shape of a linearly decreasing distributed load is triangular, one may write:

$$R = \frac{1}{2} W_{lip} q_{max}$$

Equation C-1

Which implies:

$$q_{max} = \frac{2R}{W_{lip}}$$

Equation C-2

With the slope and *y*-intercept of the line *q(x)*, one may write its equation:

$$q(x) = q_{max} - \left(\frac{q_{max}}{W_{lip}} \right) x = \frac{2R}{W_{lip}} - \left(\frac{2R}{(W_{lip})^2} \right) x \qquad 0 \le x < W_{lip}$$

Equation C-3

This is the equation for the value of the load at any point between the edge of the lip and its intersection with the filter wall.

Determination of the Internal Shear Function and the Internal Moment Function

Note that in this equation, only the *magnitude* of the load is considered. Ordinarily in beam theory, an upward load is considered negative; this consideration will be taken into account by defining the internal shear function, *v(x)*, and internal moment function, *M(x)*, as positive when acting in the same direction as the support reactions shown in Figure 3-5 above.

Integrating the load function with respect to *x* yields:

$$v(x) = q_{max} x - \left(\frac{q_{max}}{2W_{lip}} \right) x^2 + K \qquad 0 \le x < W_{lip}$$

Equation C-4

In order for equilibrium to be maintained, internal shear at the free end of the lip must be zero. That is:

v(0) = 0.

This implies that *K*, the constant of integration = 0, which leaves:

$$v(x) = q_{max} x - \left(\frac{q_{max}}{2W_{lip}} \right) x^2 \qquad 0 \le x < W_{lip}$$

Equation C-5

This is the equation for the value of the shear at any point between the edge of the lip and its intersection with the filter wall.

Integrating the shear function with respect to x yields:

$$M(x) = \frac{q_{max} x^2}{2} - \left(\frac{q_{max}}{6W_{lip}} \right) x^3 + K_2 \qquad 0 \le x < W_{lip}$$

Equation C-6

Applying the constraint that, at the free end of the lip, internal moment must be zero:

$M(0) = 0$.

This implies that $K_2 = 0$, leaving:

$$M(x) = \frac{q_{max} x^2}{2} - \left(\frac{q_{max}}{6W_{lip}} \right) x^3 \qquad 0 \le x < W_{lip}$$

Equation C-7

This is the equation for the value of the moment at any point between the edge of the lip and its intersection with the filter wall.

Determination of Magnitude and Location of Maximum Moment

Now, one may demonstrate that the moment function is monotonically increasing on the interval

$0 \le x < W_{lip}$ by applying a first derivative test. Since the first derivative of a function is the slope of its graph, if the derivative of the moment function is positive on the interval $0 \le x < W_{lip}$, the moment function must be constantly increasing on the same interval.

Conveniently, the shear function *is* the derivative of the moment function. To demonstrate that the shear function is positive, we begin by assuming the opposite and performing algebraic manipulation until we reach a known contradiction:

$$q_{max} x - \frac{q_{max}}{2W_{lip}} x^2 \le 0$$

Equation C-8

Since we know that this function is equal to zero at $x = 0$, we define x as non-zero for purposes of this proof. We may then divide both sides of this equation by $q_{max}x$ to yield:

$$1 - \frac{x}{2W_{lip}} \leq 0$$

Equation C-9

Multiplying both sides by $2W_{lip}$ and adding $-x$ to both sides yields:

$$2W_{lip} \leq x$$

Equation C-10

The interval under consideration is $0 < x < W_{lip}$. Therefore, $2W_{lip}$ cannot be less than or equal to x, and we have demonstrated our original assumption to be false by *reductio ad absurdum*.

The moment function therefore achieves its maximum at $x = W_{lip}$, which reveals a formula for maximum moment:

$$M_{max} = \frac{q_{max}\left(W_{lip}\right)^2}{2} - \left(\frac{q_{max}}{6W_{lip}}\right)\left(W_{lip}\right)^3 = \frac{q_{max}\left(W_{lip}\right)^2}{3}$$

Equation C-11

APPENDIX D: Tabulated Results

NOTE: *W = Width, T = Thickness, L = Distance Between Supports, P_{max} = Load at Rupture, M_{max} = Moment at Rupture, R = Modulus of Rupture*

Position	Recipe #	W (mm)	T (mm)	L (mm)	P_{max} (N)	M_{max} (Nmm)	R (MPa)
A	1	22	22	95	214.125	5.1E+03	2.9
A	2	22	22	95	229.467	5.4E+03	3.1
A	3	21	22	95	132.628	3.1E+03	1.9
A	4	21	22	95	172.084	4.1E+03	2.4
A	5	21	22	95	76.336	1.8E+03	1.1
A	6	21	22	95	84.567	2.0E+03	1.2
A	7	21	22	95	378.230	9.0E+03	5.3
A	8	21	22	95	456.163	1.1E+04	6.4
A	9	22	22	95	301.077	7.2E+03	4.0
A	10	21	22	95	377.176	9.0E+03	5.3
A	11	21	22	95	212.262	5.0E+03	3.0
A	12	22	22	95	178.166	4.2E+03	2.4
A	13	21	21	95	601.839	1.4E+04	9.3
A	14	20	21	95	459.274	1.1E+04	7.4
B	1	21	22	95	210.078	5.0E+03	2.9
B	2	22	22	95	222.943	5.3E+03	3.0
B	3	21	21	95	144.947	3.4E+03	2.2
B	4	21	22	95	142.246	3.4E+03	2.0
B	5	20	22	95	116.893	2.8E+03	1.7
B	6	22	22	95	70.294	1.7E+03	0.9
B	7	21	21	95	310.750	7.4E+03	4.8
B	8	22	22	95	306.828	7.3E+03	4.1
B	9	21	22	95	235.065	5.6E+03	3.3
B	10	22	23	95	255.664	6.1E+03	3.1
B	11	21	21	95	207.029	4.9E+03	3.2
B	12	21	21	95	178.778	4.2E+03	2.8
B	13	21	21	95	429.820	1.0E+04	6.6
B	14	20	20	95	448.822	1.1E+04	8.0
C	1	22	22	95	271.545	6.4E+03	3.6
C	2	22	22	95	146.392	3.5E+03	2.0
C	3	22	22	95	191.454	4.5E+03	2.6
C	4	21	22	95	166.849	4.0E+03	2.3
C	5	21	21	95	107.031	2.5E+03	1.6

C	6	20	21	95	114.126	2.7E+03	1.8
C	7	21	21	95	212.782	5.1E+03	3.3
C	8	21	22	95	342.325	8.1E+03	4.8
C	9	21	22	95	224.837	5.3E+03	3.2
C	10	21	22	95	245.361	5.8E+03	3.4
C	11	20	21	95	196.891	4.7E+03	3.2
C	12	22	22	95	150.405	3.6E+03	2.0
C	13	19	21	95	417.918	9.9E+03	7.1
C	14	21	21	95	258.478	6.1E+03	4.0
D	1	22	22	95	192.659	4.6E+03	2.6
D	2	22	22	95	252.236	6.0E+03	3.4
D	3	22	22	95	186.216	4.4E+03	2.5
D	4	22	22	95	174.449	4.1E+03	2.3
D	5	21	22	95	89.321	2.1E+03	1.3
D	6	22	22	95	102.153	2.4E+03	1.4
D	7	21	22	95	372.484	8.8E+03	5.2
D	8	21	22	95	338.401	8.0E+03	4.7
D	9	22	22	95	210.477	5.0E+03	2.8
D	10	22	22	95	248.198	5.9E+03	3.3
D	11	22	21	95	176.410	4.2E+03	2.6
D	12	22	22	95	127.043	3.0E+03	1.7
D	13	21	22	95	344.166	8.2E+03	4.8
D	14	22	22	95	292.093	6.9E+03	3.9
E	1	21	22	95	303.547	7.2E+03	4.3
E	2	21	22	95	284.013	6.7E+03	4.0
E	3	21	21	95	221.075	5.3E+03	3.4
E	4	21	22	95	220.720	5.2E+03	3.1
E	5	21	21	95	144.803	3.4E+03	2.2
E	6	20	21	95	149.151	3.5E+03	2.4
E	7	21	21	95	418.388	9.9E+03	6.4
E	8	21	22	95	346.914	8.2E+03	4.9
E	9	21	21	95	247.055	5.9E+03	3.8
E	10	21	22	95	202.084	4.8E+03	2.8
E	11	22	22	95	180.930	4.3E+03	2.4
E	12	21	22	95	141.153	3.4E+03	2.0
E	13	20	21	95	437.048	1.0E+04	7.1
E	14	21	21	95	291.592	6.9E+03	4.5
F	1	22	22	95	271.405	6.4E+03	3.6

F	2	21	22	95	245.941	5.8E+03	3.4
F	3	21	22	95	214.806	5.1E+03	3.0
F	4	21	23	95	204.818	4.9E+03	2.6
F	5	*Broken on Actuator, No Data Recorded*					
F	6	21	22	95	142.419	3.4E+03	2.0
F	7	21	21	95	458.940	1.1E+04	7.1
F	8	21	22	95	267.718	6.4E+03	3.8
F	9	22	22	95	233.000	5.5E+03	3.1
F	10	21	22	95	263.327	6.3E+03	3.7
F	11	21	22	95	156.357	3.7E+03	2.2
F	12	21	22	95	162.742	3.9E+03	2.3
F	13	21	22	95	471.270	1.1E+04	6.6
F	14	22	22	95	218.134	5.2E+03	2.9
G	1	22	22	95	150.076	3.6E+03	2.0
G	2	22	22	95	171.864	4.1E+03	2.3
G	3	20	22	95	161.426	3.8E+03	2.4
G	4	21	23	95	157.525	3.7E+03	2.0
G	5	21	21	95	101.037	2.4E+03	1.6
G	6	21	22	95	105.536	2.5E+03	1.5
G	7	20	22	95	309.254	7.3E+03	4.6
G	8	21	22	95	289.224	6.9E+03	4.1
G	9	21	21	95	249.117	5.9E+03	3.8
G	10	21	22	95	287.436	6.8E+03	4.0
G	11	20	21	95	162.467	3.9E+03	2.6
G	12	21	21	95	145.329	3.5E+03	2.2
G	13	22	22	95	499.009	1.2E+04	6.7
G	14	21	21	95	379.082	9.0E+03	5.8
H	1	22	22	95	83.177	2.0E+03	1.1
H	2	23	23	95	85.734	2.0E+03	1.0
H	3	21	21	95	82.047	1.9E+03	1.3
H	4	21	22	95	62.687	1.5E+03	0.9
H	5	21	22	95	41.127	9.8E+02	0.6
H	6	21	22	95	48.552	1.2E+03	0.7
H	7	21	22	95	176.538	4.2E+03	2.5
H	8	22	21	95	207.664	4.9E+03	3.1
H	9	22	22	95	142.610	3.4E+03	1.9
H	10	21	22	95	173.222	4.1E+03	2.4
H	11	21	21	95	139.326	3.3E+03	2.1

H	12	22	22	95	112.601	2.7E+03	1.5
H	13	22	22	95	451.719	1.1E+04	6.0
H	14	21	21	95	311.390	7.4E+03	4.8
I	1	22	22	95	144.869	3.4E+03	1.9
I	2	22	23	95	187.604	4.5E+03	2.3
I	3	22	21	95	153.866	3.7E+03	2.3
I	4	21	22	95	133.198	3.2E+03	1.9
I	5	20	22	95	103.130	2.4E+03	1.5
I	6	21	22	95	79.356	1.9E+03	1.1
I	7	22	22	95	360.617	8.6E+03	4.8
I	8	21	23	95	291.464	6.9E+03	3.7
I	9	22	21	95	201.293	4.8E+03	3.0
I	10	21	22	95	234.627	5.6E+03	3.3
I	11	21	21	95	188.621	4.5E+03	2.9
I	12	21	21	95	134.315	3.2E+03	2.1
I	13	21	21	95	397.295	9.4E+03	6.1
I	14	21	21	95	328.788	7.8E+03	5.1
I thin	4thin	*Broken in Kiln, No Data Recorded*					
I med	4med	23	17	95	80.509	1.9E+03	1.7
II med	4med	23	17	95	95.816	2.3E+03	2.1
II thin	4thin	23	11	95	20.669	4.9E+02	1.1
III thin	4thin	23	10	95	32.970	7.8E+02	2.0
III med	4med	22	17	95	99.899	2.4E+03	2.2
IV thin	4thin	22	11	95	29.471	7.0E+02	1.6
IV med	4med	22	16	95	92.725	2.2E+03	2.3
V thin	4thin	23	11	95	28.739	6.8E+02	1.5
V med	4med	23	17	95	68.750	1.6E+03	1.5
VI thin	4thin	24	11	95	18.619	4.4E+02	0.9
VI med	4med	23	17	95	89.823	2.1E+03	1.9
VII thin	4thin	23	10	95	18.093	4.3E+02	1.1
VII med	4med	23	17	95	98.234	2.3E+03	2.1
VIII thin	4thin	23	10	95	13.887	3.3E+02	0.9
VIII med	4med	*Dropped and Broken, No Data Recorded*					
IX thin	4thin	23	10	95	19.093	4.5E+02	1.2
IX med	4med	23	17	95	62.197	1.5E+03	1.3
X thin	4thin	23	11	95	23.391	5.6E+02	1.2
X med	4med	23	17	95	53.708	1.3E+03	1.2

APPENDIX E: Description of Statistical Tests

Small-Sample Tests About (μ_a - μ_b) When Populations *a* and *b* Possess Unequal Variances

In order to determine whether a sample set possesses a characteristic in greater measure than another sample set, one may begin by positing a null hypothesis about the difference between the population means of said characteristic from each set. In this thesis, one posits a null hypothesis for the difference in the mean bending strength of two recipes, *a* and *b*:

$$H_0 : \mu_a - \mu_b = 0$$

where μ_a and μ_b represent the mean modulus of rupture for the entire population of recipes *a* and *b*, respectively. This hypothesis suggests that there is no difference between the moduli of rupture. One wishes to reject this null hypothesis, and instead demonstrate an alternative hypothesis, namely:

$$H_a : \mu_a - \mu_b > 0 \rightarrow \mu_a > \mu_b$$

To test the hypothesis, one first calculates the appropriate test statistic. Mendenhall and Sincich (2007, p. 361) provide the following test statistic for a small-sample test about the difference between means from two populations with unequal variances:

$$T = \frac{\overline{y_a} - \overline{y_b}}{\sqrt{\frac{s_a^2 + s_b^2}{n}}},$$

where:

$\overline{y_x}$ is the mean of the samples of population *x,*

s_x is the standard deviation of the samples of population *x*, and

n is the number of samples in each sample set.

With the test statistic calculated, one then compares this statistic to the well-known *T*-distribution at the desired level of confidence. Mendenhall and Sincich (2007, p. 910) provide a table of values for t_α, where (1-α)100% = the confidence level of one's test. In order to enter the table, one must compute the degrees of freedom, *v*, of their sample set. Mendenhall and Sincich (2007, p. 361) provide the following formula:

$$\nu = 2(n-1)$$

For all but one recipe, nine samples were successfully tested. For recipe #5, only 8 samples were successfully tested. Mendenhall and Sincich (2007, p. 361) provide alternate formulas for computing the test statistic and degrees of freedom for sample sets *a* and *b* of unequal size:

$$T = \frac{\overline{y_a} - \overline{y_b}}{\sqrt{\frac{s_a^2}{n_a} + \frac{s_b^2}{n_b}}};$$

$$\nu = \left\lfloor \frac{\left(s_a^2 / n_a + s_b^2 / n_b\right)^2}{\left[\frac{\left(s_a^2 / n_a\right)^2}{n_a - 1} + \frac{\left(s_b^2 / n_b\right)^2}{n_b - 1}\right]} \right\rfloor$$

Equipped thus with the test statistic and value of t_α, one may state with (1-α)100% confidence that $\mu_3 > \mu_1$ if T > t_α.

Small-Sample Test of $\mu > D$

In order to determine whether a population mean exceeds some value, *D*, one follows a similar procedure. First, define the null and alternative hypotheses:

$$H_0 : \mu = D$$
$$H_a : \mu > D$$

Then compute the lower bound of the population mean for a given level of confidence using the following equation:

$$T = \overline{y} - t_{\alpha/2}\left(\frac{s}{\sqrt{n}}\right),$$

where $t_{\alpha/2}$ is the *T*-value corresponding to a confidence level of (1-α)100%.

One may now state with (1-α)100% confidence that μ > D if $T > D$.

Determination of the Probability $P(R < D)$

To determine the probability that a given value from a population, *R*, is less than some predetermined value, *D*, one first computes the *Z-score* of the value, *D*, according to:

$$Z = \frac{\overline{y} - D}{s}.$$

One may then determine from tabulated values of the normal distribution the fraction of area under the normal curve lying below this calculated *Z-score*. For this thesis, a Java applet created by David Lane, Associate Professor in the Departments of Psychology, Statistics, and Management at Rice University, was used in lieu of tabulated values (2008).

References

Alethia Environmental. (2001a). *Investigation of the Potters for Peace Colloidal Silver Impregnated Ceramic Filter - Report 1: Intrinsic Effectiveness* (USAID Purchase Order Number 524-0-00-01-00014-5362). Allston, MA: Lantagne, D.S.

Alethia Environmental. (2001b). *Investigation of the Potters for Peace Colloidal Silver Impregnated Ceramic Filter - Report 2: Field Investigations* (USAID Purchase Order Number 524-0-00-01-0014-5362). Allston, MA: Lantagne, D.S.

American Society of Testing and Materials. (2006). *C368-88 Standard Test Method for Impact Resistance of Ceramic Tableware.* Retrieved May 15, 2010, from http://subscriptions.techstreet.com.libproxy.mit.edu/products/show/137099

American Society of Testing and Materials. (2006). *C674-88 Standard Test Method for Flexural Properties of Ceramic Whitewares.* Retrieved May 15, 2010, from http://subscriptions.techstreet.com.libproxy.mit.edu/products/show/137106

Beer, F. P., Johnston Jr., E. R., & Eisenberg, E. R. (2004). *Vector Mechanics for Engineers, Statics: Seventh Edition.* New York: McGraw-Hill.

Bloem, Sophie C.; van Halem, Doris; Sampson, Mickey L.; Huoy, Laing-Shun; Heijman, Bas. (2009). Silver Impregnated Pot Filter: Flow Rate versus the Removal Efficiency of Pathogens. *Water Environment Federation Disinfection 2009: International Ceramic Pot Filter Workshop*. Delft University of Technology; The Netherlands, United Nations Educational, Scientific, and Cultural Organization International Institute for Hydraulic and Environmental Engineering; The Hague, Resource Development International – Cambodia.

Central Intelligence Agency. (2009, November 20). *CIA - The World Factbook -- Ghana*. Retrieved December 4, 2009, from https://www.cia.gov/library/publications/the-world-factbook/geos/gh.html

Cook, R. D., Malkus, D. S., & Plesha, M. E. (1989). *Concepts and Applications of Finite Element Analysis: Third Edition.* New York: John Wiley & Sons, Inc.

Desmyter, D., Adagwine, A. P., Ibrahim, S., Jackson, M. K., & Murcott, S. E. (2008). Monitoring and Evaluation of 1,000 Households receiving ceramic Pot (Kosim) Filters after an Emergency Flood Mass Distribution in Northern Ghana. *Water Environment Federation Disinfection 2009: International Ceramic Pot Filter Workshop*. Cambridge, Massachusetts Institute of Technology.

DoultonUSA. (2010). *History of Doulton Water Filters*. Retrieved March 1, 2010, from Doulton Water Filter Ceramic Candle and Cartridge Technologies: http://doultonusa.com/HTML%20pages/history.htm

Fitzpatrick, D. (2008). *Efficacy of Gravity-Fed Chlorination System for Community-Scale Water Disinfection in Northern Ghana.* Master's thesis, Civil and Environmental Engineering, Massachusetts Institute of Technology, Cambridge.

Ghana Statistical Service. (2005). 2000 Population and Housing Census: Analysis of District Data and Implications for Planning - Northern Region. Ghana Statistical Service.

Johnson, S. (2007). *Health and Water Quality Monitoring of Pure Home Water's Ceramic Filter Dissemination in the Northern Region of Ghana.* Master's thesis, Civil and Environmental Engineering, Massachusetts Institute of Technology, Cambridge.

Kallman, E., Smith, J., & Oyanedel-Craver, V. (2009). Field Evaluation of Locally Produced Silver-Impregnated Ceramic Filters for Point-Of-Use Water Purification in San Mateo Ixtatan, Guatemala. *Water Environment Federation Disinfection 2009: International Ceramic Pot Filter Workshop*. Richmond, University of Virginia; Kingston, University of Rhode Island.

Klarman, M. (2009). *Investigation of Ceramic Pot Filter Design Variables.* Master's thesis, Public Health, Emory University, Atlanta, Georgia.

Lane, D. (2008, November 26). *Z table - Normal Distribution*. Retrieved April 13, 2010, from David Lane: http://davidmlane.com/hyperstat/z_table.html

Mendenhall, W., & Sincich, T. (2007). *Statistics for Engineering and the Sciences: Fifth Edition.* Upper Saddle River, New Jersey: Prentice Hall, Inc.

Miller (2010). *Optimizing Performance of Ceramic Pot Filters in Northern Ghana and Modeling Flow through Paraboloid-Shaped Filters*. Master's thesis, Civil and Environmental Engineering, Massachusetts Institute of Technology, Cambridge.

Murcott, S. (2009, September 11). *Expanding Pure Home Water's Water/Sanitation/Hygiene Social Enterprise in Northern Ghana.* 1.782 Environmental Engineering Master's of Engineering Project. [PowerPoint lecture presented in Bechtel Lecture Hall, Room 1-390, Massachussets Institute of Technology].

Nath KJ, Bloomfield SF, Jones M (2006). *Household water storage, handling and point-of-use treatment.* A review commissioned by the International Scientific Forum on Home Hygiene; published on http://www.ifh-homehygiene.org

Nidec-Shimpo America. (2009, November). *kilnmanual.pdf.* Retrieved April 13, 2010, from Shimpo Ceramics: http://www.shimpoceramics.com/pdf/kilnmanual.pdf

Niven, R. (2005). *Investigation of Silver Electrochemistry Water Disinfection Applications.* Montreal: McGill University, Department of Civil Engineering.

Oyanedel-Craver, V., & Smith, J. (2008). Sustainable Colloidal-Silver Impregnated Ceramic Filter for Point-of-Use Water Treatment. *Environmental Science and Technology* , 927-33.

Potters for Peace. (2006). *Filters*. Retrieved March 1, 2010, from Potters for Peace: http://www.pottersforpeace.org/?page_id=9

Pure Home Water. (2009). *Home*. Retrieved March 1, 2010, from Pure Home Water: http://purehomeh2o.com/2.html

Rayner, J. (2009). *Current Practices in Manufacturing of Ceramic Pot Filters for Water Treatment.* Master's Thesis, Loughborough University, Civil and Building Engineering, Leicestershire, UK.

United Nations. (2009). *Millennium Development Goals Report* (Sales Number E.09.I.12). New York: United Nations Department of Economic and Social Affairs.

United Nation's International Children's Fund. (2007). *State of the World's Children 2008: Child Survival* (Sales Number E.08.XX.1). New York: UNICEF.

United Nations International Children's Fund. (2007). *Use of Ceramic Water Filters in Cambodia.* UNICEF: Brown, Joe; Sobsey, Mark; Proum, Sorya.

University of Ljubljana. (2003). *Lecture 8.4.2 : Plate Girder Behaviour and Design II*. Retrieved April 17, 2010, from Chair for Metal Structures: http://www.fgg.uni-lj.si/kmk/ESDEP/master/wg08/l0420.htm

Van Calcar, J. (2006). *Collection and Representation of GIS Data to Aid Household Water Treatment and Safe Storage Technology Implementation in the Northern Region of Ghana.* Master's thesis, Civil and Environmental Engineering, Massachusetts Institute of Technology, Cambridge.

van Halem, D. (2006). *Ceramic silver impregnated pot filters for household drinking water treatment in developing countries.* Master's thesis, Civil Engineering and Geosciences, Delft University of Technology.

van Halem, D., van der Laan, H., Heijman, S. G., van Dijk, J. C., & Amy, G. L. (2009). Assessing the sustainability of the silver-impregnated ceramic pot filter for low-cost household drinking water treatment. *Physics and Chemistry of the Earth* , 36-42.

Whiteware (2010). In *Encyclopaedia Britannica*. Retrieved March 26, 2010, from Encyclopaedia Britannica Online: http://www.britannica.com/EBchecked/topic/642810/whiteware

World Health Organization. (1997). *Guidelines for Drinking-water Quality, Second Edition, Volume III: Surveillance and Control of Community Water Supplies*. Geneva: WHO Press.

World Health Organization. (2008). *Guidelines for Drinking-water Quality, Third Edition Incorporating the First and Second Addenda: Volume 1 Recommendations*. Geneva: WHO Press.

World Health Organization. (2006). *Mortality Country Fact Sheet 2006.* Retrieved February 17, 2010, from WHO Statistical Information System: http://www.who.int/whosis/mort/profiles/mort_afro_gha_ghana.pdf

World Health Organization. (2004). *Water, sanitation and hygiene links to health*. Retrieved February 17, 2010, from WHO: http://www.who.int/water_sanitation_health/publications/facts2004/en/index.html

World Health Organization/United Nations International Children's Fund Joint Monitoring Programme for Water Supply and Sanitation. (2008). *Progress on Drinking Water and Sanitation: Special Focus on Sanitation.* New York: UNICEF; Geneva, Switzerland: WHO.

Ziff, S. (2009). *Siphon Filter Assessment for Northern Ghana.* Master's thesis, Civil and Environmental Engineering, Cambridge: Massachusetts Institute of Technology.